SECURITY INFORMATION

~~CONFIDENTIAL~~

Copy 228
RM L52C10

NACA RM L52C10

TECH LIBRARY KAFB, NM
0143837

NACA

RESEARCH MEMORANDUM

USE OF AN AERODYNAMICALLY PULSED ALL-MOVABLE HORIZONTAL TAIL TO OBTAIN LONGITUDINAL CHARACTERISTICS OF ROCKET-POWERED MODELS IN FREE FLIGHT AND SOME INITIAL RESULTS FROM AN ARROW-WING-BODY-TAIL CONFIGURATION

By Warren Gillespie, Jr. and Albert E. Dietz

Langley Aeronautical Laboratory
Langley Field, Va.

[redacted]

This material contains information affecting the [redacted] of the [redacted], U.S.C., Secs. 793 and 794, the transmission or revelation of which in any [redacted] to an unauthorized person is prohibited by law.

NATIONAL ADVISORY COMMITTEE
FOR AERONAUTICS

WASHINGTON
May 19, 1952

~~CONFIDENTIAL~~

PERMANENT RECORD

Classification cancelled (or changed to Unclassified)

By Authority: NASA Tech Pub Announcement #98
(OFFICER AUTHORIZED TO CHANGE)

By ..... 26 Mar 56

NK

GRADE OF OFFICER MAKING CHANGE)

7 Apr 61
DATE

TECH LIBRARY KAFB, NM
0143839

NATIONAL ADVISORY COMMITTEE FOR AERONAUTICS

RESEARCH MEMORANDUM

USE OF AN AERODYNAMICALLY PULSED ALL-MOVABLE HORIZONTAL TAIL TO OBTAIN LONGITUDINAL CHARACTERISTICS OF ROCKET-POWERED MODELS IN FREE FLIGHT AND SOME INITIAL RESULTS FROM AN ARROW-WING-BODY-TAIL CONFIGURATION

By Warren Gillespie, Jr. and Albert E. Dietz

SUMMARY

The application of an aerodynamically pulsed horizontal tail to determine experimentally the longitudinal aerodynamic characteristics of a rocket-powered model in free flight has been studied. The all-movable horizontal tail was mass-balanced about a hinge line located aft of the tail aerodynamic center. A square-wave pulse was continuously generated when the tail automatically flipped between stop settings.

A graphical procedure for determining the pitching response was applied to an assumed rocket model of a swept-wing airplane configuration to investigate the feasibility of aerodynamic pulsing. Effects of varying the model static margin, downwash at the tail, longitudinal inertia, and inertia and weight together upon the pitching response were investigated.

The technique was then applied experimentally to a rocket-powered model having an arrow wing of 67.5° leading-edge sweep, aspect ratio 1.85, body of fineness ratio 11.1, a ratio of body diameter to wing span of 0.23, and an unswept horizontal tail of aspect ratio 2.3. The Mach number range covered during the time the model continually pulsed was 0.69 to 1.00.

Both preflight calculations and flight-test data showed that downwash from the wing increases the angle of attack at which the tail will flip. The steady-state angle-of-attack response to a unit tail deflection should, therefore, be slightly greater than the required angle of attack to flip the tail in order to insure that a continuous pitching oscillation will develop.

Data were obtained on the drag due to lift, lift-curve slope for the range of lift coefficient 0.2 to -0.4, the tail effectiveness, and downwash at tail flip angles of the test model.

INTRODUCTION

Two types of pulsing methods are currently used to obtain longitudinal aerodynamic characteristics from pitching oscillations of free-flight models. One of these methods employs power-driven mechanisms within the fuselage to drive movable external surfaces which act on the air stream. The other method uses small pulse rockets to disturb the model from trim. The first method limits the space available in the fuselage and places undesirable restrictions on the use of sustainer rocket motors, usually requiring large external booster rockets to attain moderately high Mach numbers. The internal pulsing mechanism is difficult to design, build, and operate. Oscillations obtained by the second method are limited by the number of pulse rockets that can be carried in the model. The time of firing of individual pulse rockets cannot be accurately controlled when delay-squib ignition is used. Data may not be obtained at the Mach number for which data are desired. The oscillations obtained by these two methods generally reduce in amplitude after each pulse so that data at maximum angles of attack are limited to the first oscillation of each pulse. In view of the limitations noted above, a third method has been considered.

The simplified pulsing method reported herein makes use of aerodynamic forces acting on an all-movable horizontal tail. This method has been developed experimentally on a simple rocket-powered model. The horizontal tail is mass-balanced and hinged aft of its aerodynamic center. A continuous pitching oscillation of approximately constant amplitude is sustained throughout the Mach number range as the tail automatically flips between stop settings as the tail lift changes direction. Calculations were first made for an assumed rocket model of the swept-wing airplane configuration of reference 1 for which the static margin, downwash, longitudinal inertia, and inertia and weight together were varied to determine the effect on the pulsing response. These calculations indicated that the method was feasible. An experimental test was conducted using a rocket-powered model having an arrow wing of 67.5° leading-edge sweep, aspect ratio 1.85, body of fineness ratio 11.1, and an unswept horizontal tail of aspect ratio 2.3.

As the model coasted from a Mach number of 1.00 to a Mach number of 0.69, the horizontal tail moved between deflections of -1.00° and 3.07° in approximately a square-wave pattern. The basic aerodynamic parameters of the configuration were determined from the pitching response of the model to the tail motion. The model was flown at the Langley Pilotless Aircraft Research Station, Wallops Island, Va.

SYMBOLS

V	forward velocity, feet per second
q	dynamic pressure, pounds per square foot
g	gravitational acceleration, 32.2 feet per second per second
M	free-stream Mach number
m	model mass, slugs
A	aspect ratio
S	wing area (wing assumed to extend to model center line)
$\bar{c}$	mean aerodynamic chord
α	angle of attack of model, degrees
α_f	angle of attack of model at tail flip, degrees
δ	horizontal-tail deflection, degrees
ϵ	effective downwash angle, degrees
t	time, seconds
I_y	moment of inertia in pitch, slug-feet square
C_L	lift coefficient
C_{L_α}	lift-curve slope for complete configuration
C_{m_α}	moment-curve slope for complete configuration
C_{L_δ}	lift-curve slope for horizontal tail alone
C_{m_δ}	moment-curve slope for horizontal tail alone
C_{D_T}	total drag coefficient
C_{D_L}	drag due to lift
C_{m_q}, $C_{m_{\dot{\alpha}}}$	model damping coefficients

A_N normal acceleration, feet per second per second

A_L longitudinal acceleration, feet per second per second

P period, seconds

X distance from the model center of gravity to the aerodynamic center of the horizontal tail, feet

The coefficients are based on wing area.

MODEL AND TEST

Figure 1 shows the geometric details of the rocket-powered flight-test configuration. Figure 2 presents photographs of the free-flight model; figure 3 shows close-up views of the horizontal tail surface and empennage; and figure 4 shows the model-booster combination in launching position. The model was made of magnesium alloy with the exception of the horizontal tail which was made of steel. The tail pivot support was enclosed by a fairing. Stops for the horizontal tail were mounted on the tip of the vertical tail. The tail was free to flip between stop settings of -1.00° and 3.07°. The model was instrumented with a four-channel telemeter which transmitted continuous records of angle of attack, total pressure, and normal and longitudinal acceleration. Horizontal-tail position was indicated by the total-pressure trace which shifted electrically a constant known amount when the tail moved from one stop position to the other.

The model was propelled to maximum speed by means of a booster. At booster burnout the model separated from the booster and coasted through the test Mach number range of approximately 1.30 to 0.69 which corresponds to a Reynolds number range (fig. 5) of approximately 13.5×10^6 to 6.3×10^6, respectively. Time histories of normal and longitudinal accelerations, total pressure, and angle of attack were obtained by standard NACA procedures, reference 2, and used in conjunction with velocity and position tracking radar and radiosonde measurements to permit evaluation of aerodynamic quantities as a function of Mach number.

TECHNIQUE

This pulse method employs a tail surface that is mass-balanced and free to rotate about an axis located aft of the tail aerodynamic-center position. The maximum rotation of the surface in either direction is

limited by a stop. Lift on the tail surface holds the surface against a stop until the pitching motion of the model induced by the tail lift reverses the lift on the tail. The tail then flips suddenly against the other stop to reverse the pitching motion. As the angle of attack builds up in the other direction, the tail flips back to the first stop position. This action continues automatically as the model coasts. The model angle of attack at which the tail should flip is a function of the effective downwash over the horizontal tail at the time of flip, the tail-wing setting before flip, and the pitching-velocity contribution to the tail angle of attack at the time of flip. Since the tail is moved by aerodynamic forces, this pulsing technique will be referred to as the "aeropulse" technique.

The aeropulse technique was applied to an assumed model of the swept-wing airplane configuration of reference 1 to check the feasibility of obtaining longitudinal aerodynamic characteristics of tail-last configurations. The results of this general analysis are presented in appendix A.

The technique was then applied to the free-flight rocket-powered model of figure 1 which was successfully flight-tested. Methods used in obtaining the longitudinal characteristics of aeropulsed models from experimental free-flight data are presented in appendix B.

ACCURACY

The limitations of the technique used are discussed in reference 2. For the flight model of the present paper, the maximum possible errors in the absolute values of Mach number, angle of attack, C_L, and C_D have been estimated. It should be emphasized that the probable error may be much less than the values presented in the following table:

	M = 1.00	M = 0.70
ΔM	±0.02	±0.02
$\Delta\alpha$, degrees	±0.50	±0.50
ΔC_L	±0.026	±0.060
ΔC_D	$\pm(0.0034 + 0.026 \sin \alpha)$	$\pm(0.0079 + 0.060 \sin \alpha)$

FREE-FLIGHT MODEL RESULTS AND DISCUSSION

Time History

A time history of the coasting portion of flight, figure 6, presents the variation of tail position, angle of attack, normal and longitudinal accelerations, and Mach number. The model separated from its booster at approximately 1.30 seconds from take-off and responded to the 3.07° tail deflection. The model did not begin immediate pulsing since the angle-of-attack response was insufficient to force the tail to flip to the opposite -1.00° stop setting. The oscillation induced by separation of the model from its booster damped as the model trim angle increased negatively with reduced Mach number.

At a trim angle of -6.1° and Mach number 1.01 the tail flipped and the automatic pitching oscillation developed. Between Mach numbers 1.01 and 0.69 a continuous square-wave pulse was generated by the tail. At the lower Mach number of 0.69 the model became unstable. The static margin was very small at this Mach number and the angle-of-attack limit for static stability was reached at the peak of the cycle.

Lift and Drag

Figure 7 presents lift coefficient plotted against angle of attack and drag coefficient at constant Mach numbers and tail settings. Figure 7(a) presents data during the aeropulsing portion of flight for both tail positions, and figure 7(b) presents data from the damped oscillation for the 3.07° tail setting.

Figure 8 shows the variation of model lift-curve slope with Mach number at constant C_L values of 0, ±0.2, and -0.4. Both increasing Mach number and increasing C_L caused an increase in C_{L_α}.

Figure 9 presents the variation of total drag coefficient with Mach number at constant lift coefficients of 0, ±0.2, and ±0.3 for both tail settings and at a lift coefficient of -0.4 for the -1.00° tail setting. The curves show a gradual drag rise starting at a Mach number of approximately 0.8.

Figure 10 presents the variation of drag due to lift with Mach number for the cases when $\alpha < 0^{\circ}$, $\delta = -1.00^{\circ}$; $\alpha > 0^{\circ}$, $\delta = 3.07^{\circ}$; and $1/57.3C_{L_\alpha}$ at $\alpha = 0^{\circ}$, $\delta = 3.07^{\circ}$ and -1.00°. Figure 11 shows that the drag due to lift for the model tested is greater than the drag due to lift for the 60° delta wing-body configuration of reference 3, which had an NACA $65_{(06)}$A006.5 airfoil section. The model of the present test

had a flat-plate wing with a pointed leading-edge section and may have experienced greater leading-edge separation than the model of reference 3. The drag due to lift is more closely approximated at subsonic speeds by the parameter $1/57.3C_{L_\alpha}$ than by $1/\pi A$ although both are presented for comparison.

Tail Effectiveness and Downwash

Figure 12 shows the variation of tail-lift effectiveness with Mach number obtained from changes in tail position which occurred at low lifting conditions. The tail effectiveness coefficient varied slightly about an average 0.01 value throughout the test range.

The effective downwash values at the tail are presented in figure 13 for the Mach numbers occurring at the time of tail flips and are plotted against the angles of attack of the wing at the time when the downwash was assumed to have been generated. The horizontal tail was displaced above the model center line. For this tail position the downwash was higher at positive angles of attack than at negative angles of attack. Downwash obtained behind a 60° delta wing at Mach number 1.53 and presented in reference 4 indicated similar results due to an elevated tail position.

CONCLUDING REMARKS

An investigation has been made of a simple aerodynamic pulsing system using an all-movable horizontal tail to obtain longitudinal aerodynamic characteristics of a rocket model in free flight. Flight test of a model having an arrow wing of 67.5° leading-edge sweep and aspect ratio 1.85 showed that, with a small amount of static margin and the tail mounted above the fuselage, a continuous pitching oscillation was sustained over an approximately constant angle-of-attack range. Reduction of data permitted an evaluation of model lift and drag, lift-curve slope, drag due to lift, tail effectiveness, and effective downwash at the tail.

Langley Aeronautical Laboratory
National Advisory Committee for Aeronautics
Langley Field, Va.

APPENDIX A

ANALYSIS OF AN ASSUMED MODEL

The longitudinal response to an aerodynamically pulsed tail surface for an assumed rocket model of the sweptback-wing airplane configuration of reference 1 was investigated by a graphical procedure. Basic aerodynamic data required in the analysis were estimated from theory and available experimental data from this and similar configurations.

Figure 14 illustrates the graphical method applied to the assumed model with center of gravity at 20 percent mean aerodynamic chord, $d\epsilon/d\alpha$ assumed equal to 0.40, tail stop limits of $\pm 3^{\circ}$, and Mach number of 0.82. The basic response to a step input of -3° tail deflection, curve A of figure 14, was first plotted. Starting at the first angle of attack at which the tail should flip, 5.0° at time equal 0.065 second, the opposite response to a step input of 3° tail deflection, curve B, was plotted. In order to cancel the -3° tail deflection after 0.065 second time and put in the response to the 3° tail deflection, curve B was added twice to the previous curve A. The response curve due to the first tail flip from -3° to 3°, curve C, was therefore obtained. At each subsequent angle of flip, this procedure was repeated; that is, the response curve to a step input, starting from the time of tail flip, was added twice to the previous resulting curve. It should be noted that all the curves must be plotted out to the same time value, otherwise the solution cannot progress. The solution should be continued until the envelopes of the final aeropulse curve approach a constant maximum amplitude. This may occur within three or four oscillations of the basic response curve A.

The aeropulse response can be obtained with better accuracy by using the following analytical solution for a step input with initial conditions taken at the model starting condition and at the time of each succeeding tail flip:

$$\alpha = \alpha_{trim} - \left(\alpha_{trim} - \alpha_o\right)e^{-bt}\left(\frac{b}{a}\sin at + \cos at\right) + \dot{\alpha}_o e^{-bt}\sin at$$

where

$$\alpha_{trim} = -\frac{\frac{mV}{57.3qS}C_{m_\delta}\delta + C_{L_\delta}\delta\, C_{m_q}\frac{\bar{c}}{2V}}{\frac{mV}{57.3qS}C_{m_\alpha} + C_{L_\alpha}C_{m_q}\frac{\bar{c}}{2V}}$$

$$b = \frac{57.3qS}{2}\left[\frac{C_{L_\alpha}}{mV} - \frac{\left(C_{m_q} + C_{m_{\dot{\alpha}}}\right)\bar{c}^2}{2VI_y}\right]$$

$$a = \left[-\frac{57.3qS}{I_y}\left(C_{m_\alpha}\bar{c} + \frac{C_{L_\alpha}C_{m_q}\ 57.3qS\bar{c}^2}{2mV^2}\right) - b^2\right]^{1/2}$$

and α_o and $\dot{\alpha}_o$ are the initial angle of attack and the angular velocity, respectively.

The effects of varying the model center-of-gravity position, downwash at the tail, longitudinal inertia, and inertia and weight together were calculated at Mach number 1.30. Figure 15 shows the effect static margin has upon the single-step and aeropulse responses. The maximum and steady-state α/δ values of figure 15(a) approach infinity as the static margin decreases to zero. The intersection of the horizontal flip-angle line with the maximum α/δ curve defines the maximum allowable static margin that will permit the continuous motion to start from rest, that is, for the particular downwash value assumed. Reference 1 indicated a value of $\frac{d\epsilon}{d\alpha}$ between 0.4 and 0.5 at Mach number 1.30; hence, the static margin for the assumed model under consideration should not be greater than approximately 5 inches at this Mach number. Figure 15(b) shows that the aeropulse system for a constant value of $\frac{d\epsilon}{d\alpha}$ equal to 0.40 should maintain a maximum angle-of-attack response which increases slightly as the static margin decreases from the limiting static margin toward zero. The period of the continuous motion is presented in figure 15(c) and is somewhat less than the natural free period of the model and increases with reduced static margin. Figure 16 shows the effect that downwash at the tail has upon the amplitude of the pitching oscillation and the period. Both the amplitude and period increase with increased downwash. Figure 17 shows the effect longitudinal inertia has upon the period and maximum α/δ for the single pulse and aeropulse when the longitudinal inertia only is varied by distributing the model mass at varying distances from a fixed center-of-gravity position and when the longitudinal inertia is varied by adding and substracting mass at equal distances from a fixed center-of-gravity position. The model was assumed to have an initial moment of inertia of 5.00 slug-feet^2. No difference in period was obtained at a given value of inertia when the mass was changed. Both curves decreased as the inertia approached zero. Unlike the period, there was considerable difference in amplitude

of the maximum values of α/δ for the single pulse and aeropulse for these two conditions. When inertia only was varied, maximum α/δ increased as inertia decreased, but a reverse trend occurred when both inertia and mass were varied together.

The larger peak angle that would result if the tail suddenly stopped flipping (see fig. 14) indicates that, once the aeropulse motion has begun, the motion will probably continue even if the actual downwash at a later time during coasting flight of a model exceeds the downwash that existed at the time the aeropulse motion began. For the assumed model under consideration, the maximum allowable downwash to start the oscillation from rest is greater at subsonic speed than at supersonic speed for the same center-of-gravity position. This condition occurs because the static margin at subsonic speed is less and the response to a unit tail deflection is greater. Application of this pulsing method to a given configuration, therefore, depends largely on the selection of a model center-of-gravity position that will permit the aeropulse motion to start automatically. If the requirements for automatic starting cannot be met by preflight adjustments to the model, use of a small pulse rocket is suggested to disturb the model initially and permit the aeropulse motion to develop.

APPENDIX B

DATA REDUCTION OF THE FLIGHT MODEL

Lift and Drag

The lift and drag coefficients were determined by transferring the normal and longitudinal accelerations measured along the body axes to the stability axes. The angle between the two sets of axes was the model angle of attack. A cross-plotting technique was used over the aeropulse region of Mach number to obtain C_{D_T} and α values at a constant C_L and Mach number. A plot of the time histories of C_L, C_{D_T}, α, and M was made on the same sheet of graph paper; constant C_L values were selected and corresponding points were projected at the same time on the C_{D_T} and α curves. The projected values at constant C_L for each item were then joined by a smooth curve throughout the time-history plot. Lines of selected constant Mach numbers were drawn perpendicular to the time axis through the C_{D_T}, and α curves determined by the projected points. Intersections of these Mach number lines and the lines of C_{D_T} and α corresponding to constant values of C_L resulted in sets of data at constant Mach numbers over the aeropulse region of Mach number. For the Mach number region of the damped oscillation, this cross-plotting technique could not be used. Plots of C_L against α and C_{D_T} were made using the method of reference 2.

Tail Effectiveness and Downwash

The tail lift effectiveness C_{L_δ} was obtained by determining the incremental shift that occurred in the normal-force-time curve (see fig. 6) each time the tail flipped. The normal-force-time curve was extrapolated to the middle of the time interval during tail flipping. This interval was very short, 0.03 second in most cases.

Effective downwash at the horizontal tail surface was determined at the start of each tail flip when the lift on the tail was assumed to be zero. The following equation was used to evaluate the downwash:

$$\epsilon = \alpha + \delta + \frac{X}{V}\left(\dot{\alpha} + 57.3\,\frac{A_N}{V}\right)$$

The downwash was assumed to originate from the wing at an earlier time, $t - \frac{X}{V}$.

REFERENCES

1. Osborne, Robert S.: High-Speed Wind-Tunnel Investigation of the Longitudinal Stability and Control Characteristics of a $\frac{1}{16}$-Scale Model of the D-558-2 Research Airplane at High Subsonic Mach Numbers and at a Mach Number of 1.2. NACA RM L9C04, 1949.

2. Gillis, Clarence L., Peck, Robert F., and Vitale, A. James: Preliminary Results from a Free-Flight Investigation at Transonic and Supersonic Speeds of the Longitudinal Stability and Control Characteristics of an Airplane Configuration with a Thin Straight Wing of Aspect Ratio 3. NACA RM L9K25a, 1950.

3. Mitcham, Grady L., Crabill, Norman L., and Stevens, Joseph E.: Flight Determination of the Drag and Longitudinal Stability and Control Characteristics of a Rocket-Powered Model of a 60° Delta-Wing Airplane from Mach Numbers of 0.75 to 1.70. NACA RM L51I04, 1951.

4. Perkins, Edward W., and Canning, Thomas N.: Investigation of Downwash and Wake Characteristics at a Mach Number of 1.53. II - Triangular Wing. NACA RM A9D20, 1949.

CONFIDENTIAL

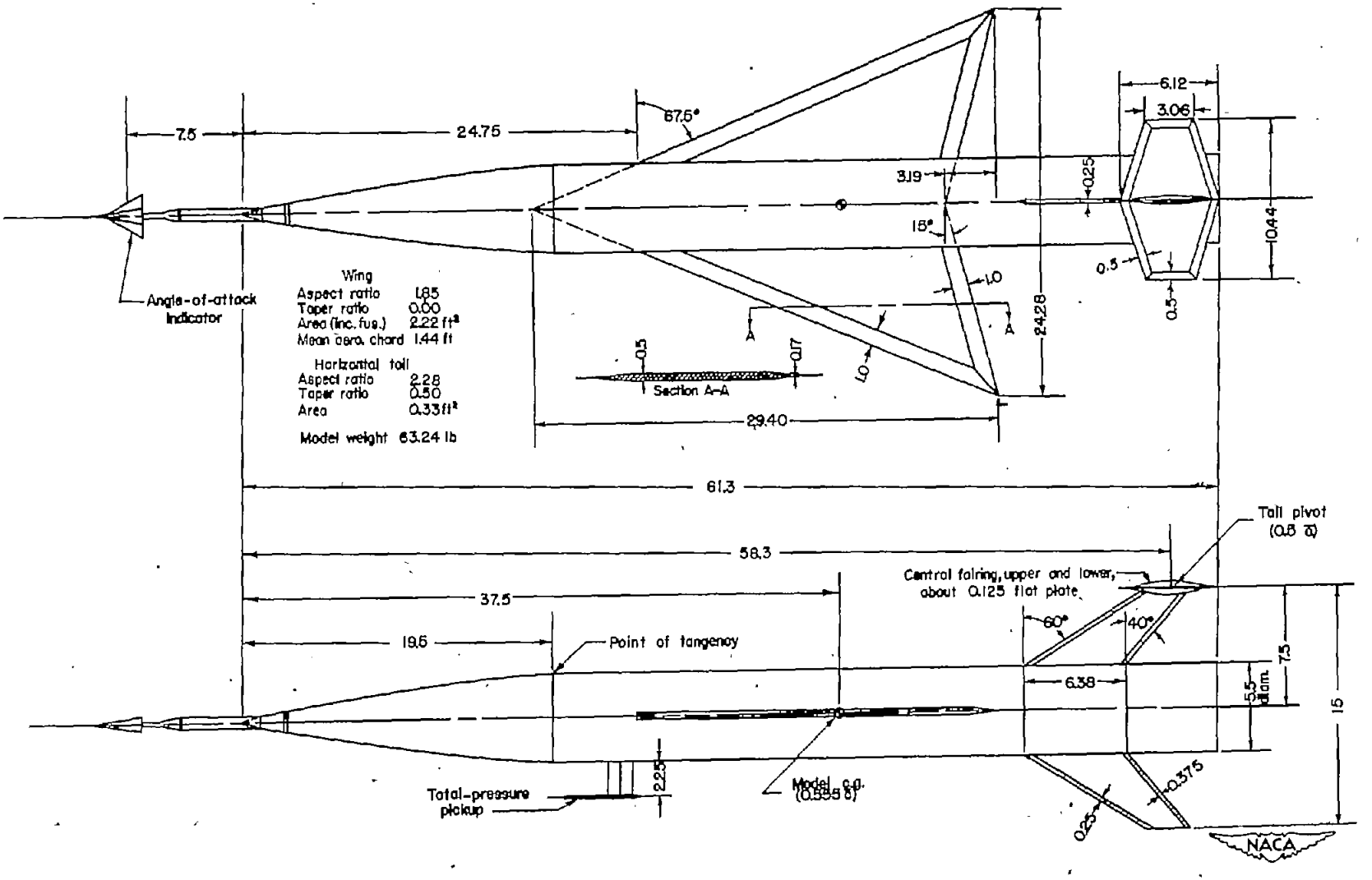

Figure 1.- Two-view drawing of test model. All dimensions in inches unless otherwise indicated.

CONFIDENTIAL

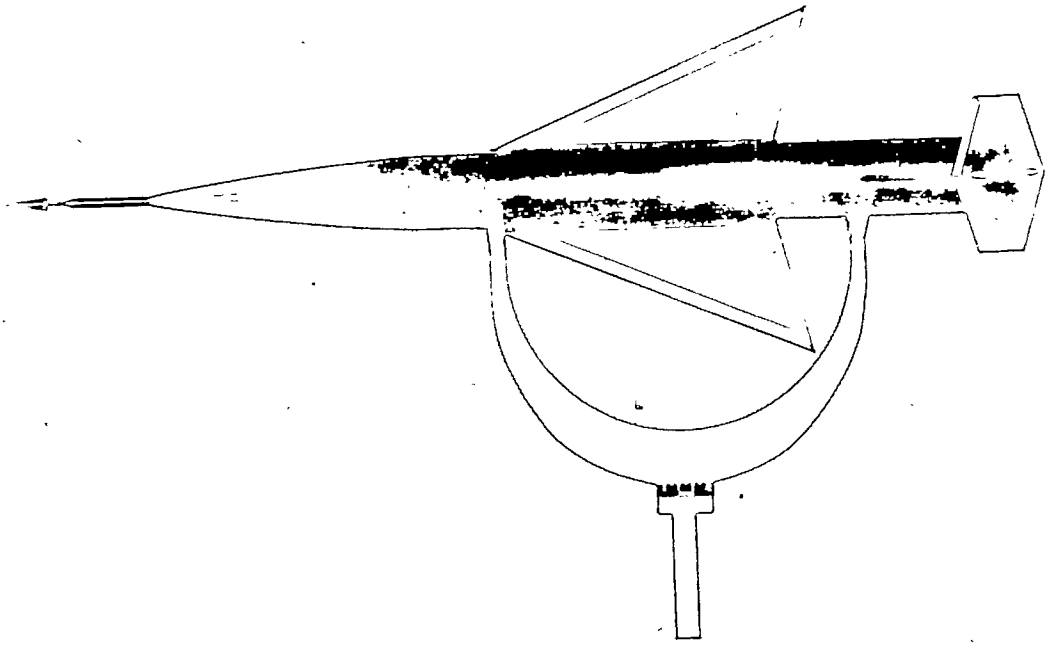

Top view

L-67414.1

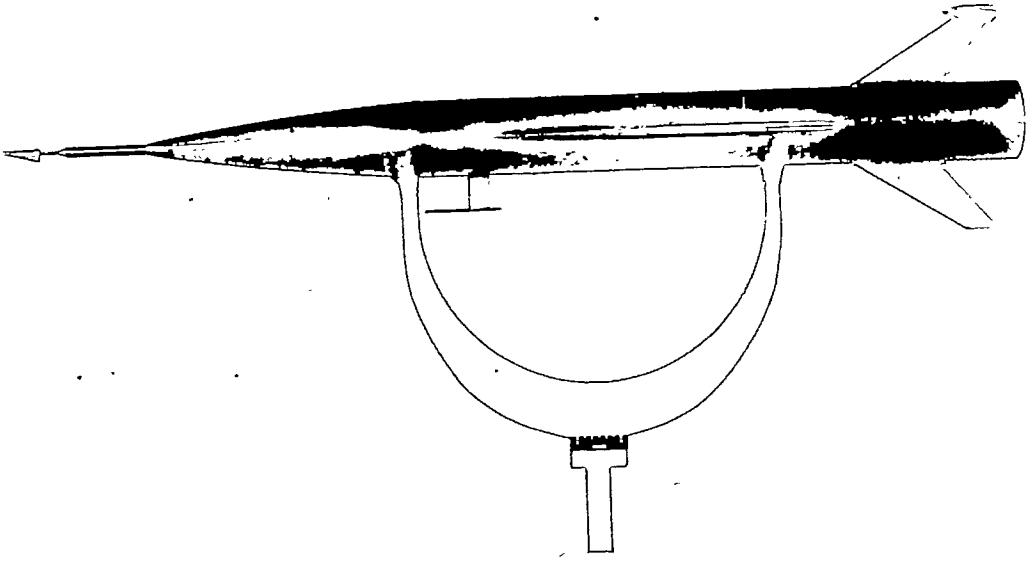

Side view

L-67415.1

Figure 2.- Photographs of test model.

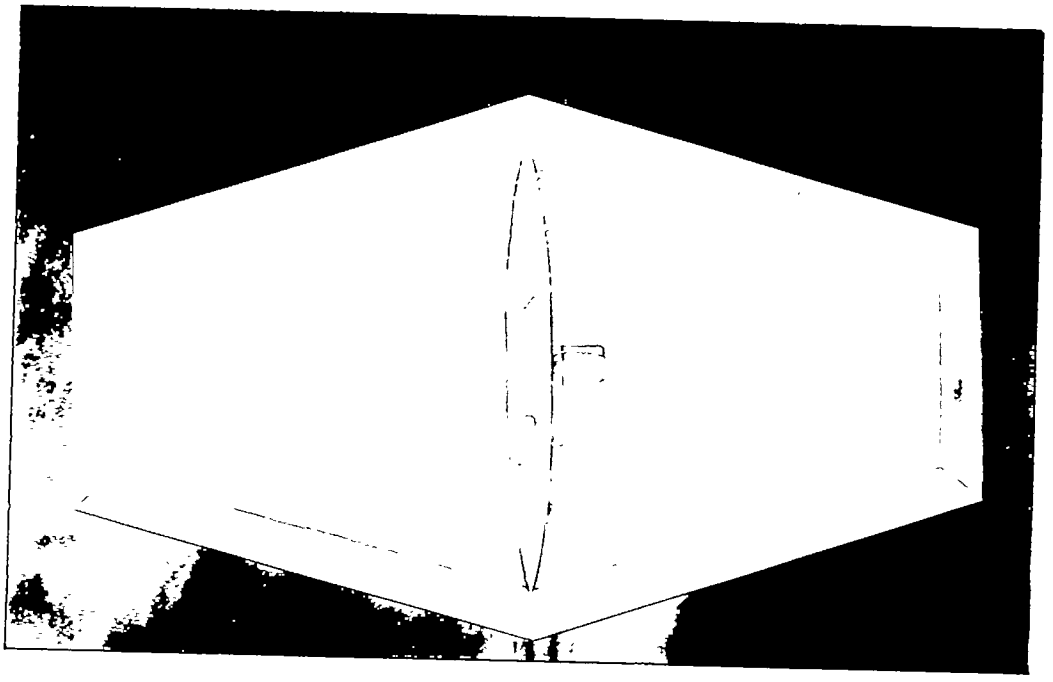

Top view

NACA
L-68613.1

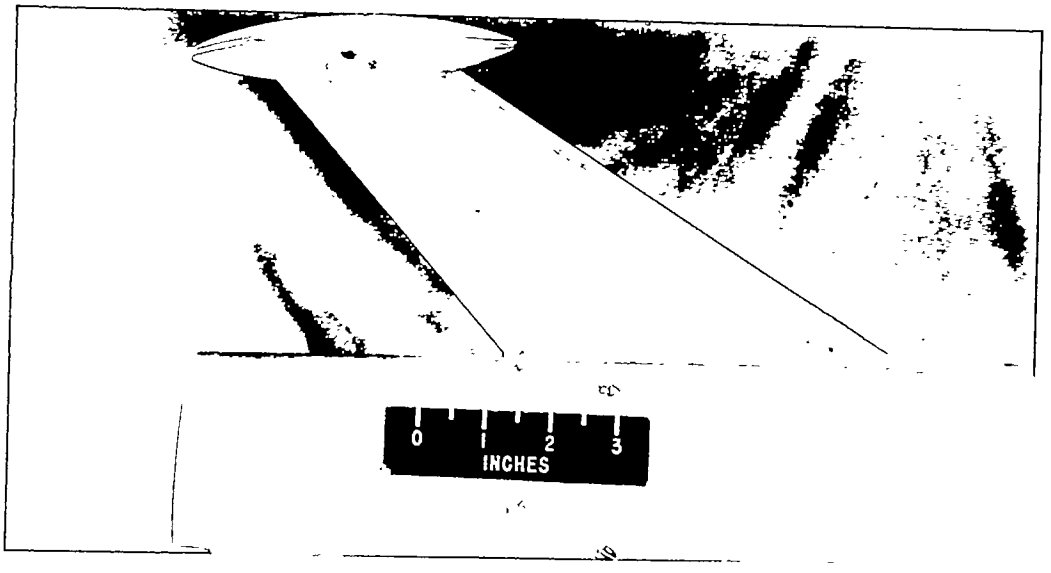

Side view

NACA
L-68614

Figure 3.- Photographs of hinged tail.

NACA
L-68754

Figure 4.- Model and booster.

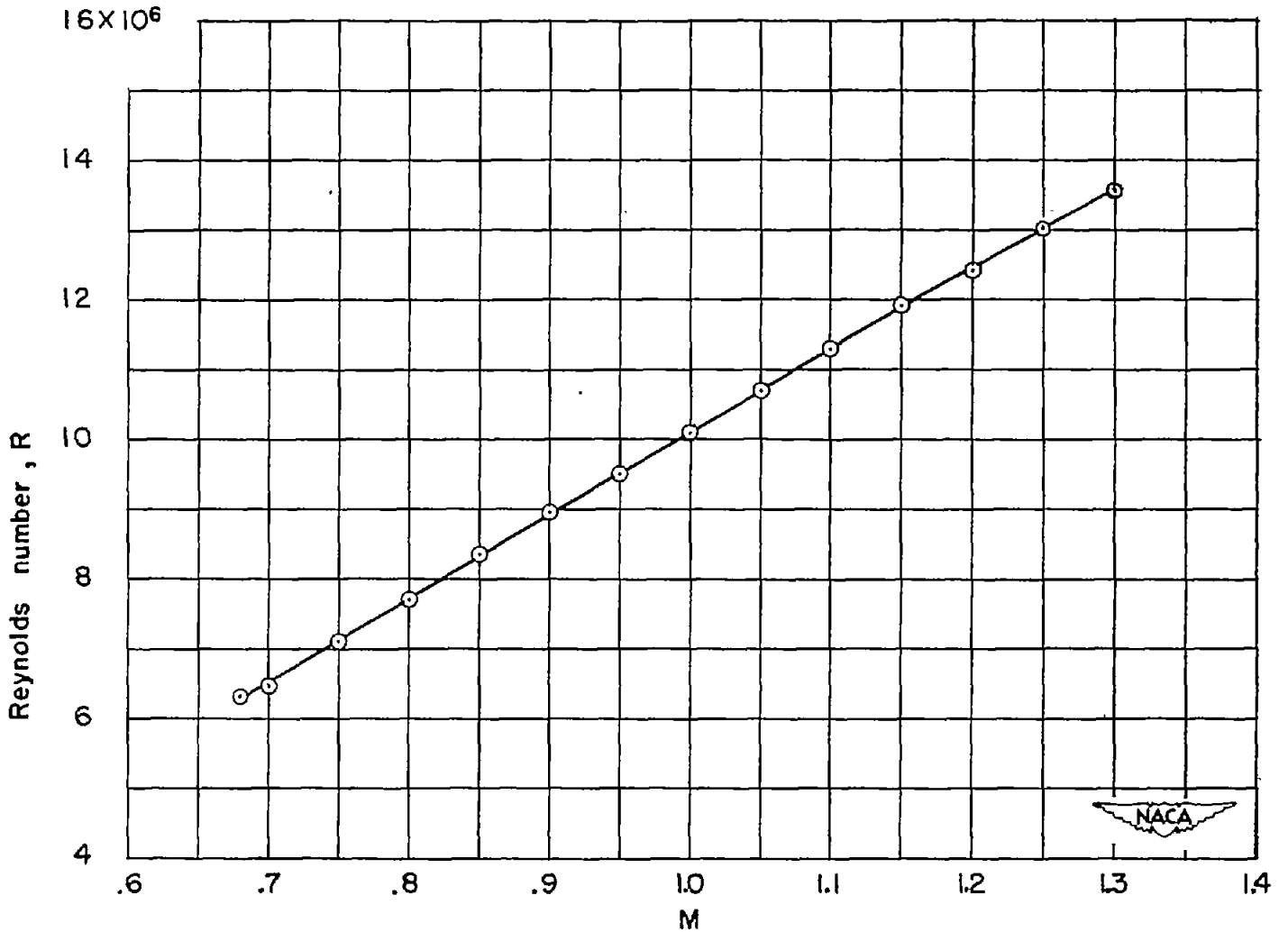

Figure 5.- Variation of test Reynolds number, based on wing mean aerodynamic chord of 1.44 feet, with Mach number.

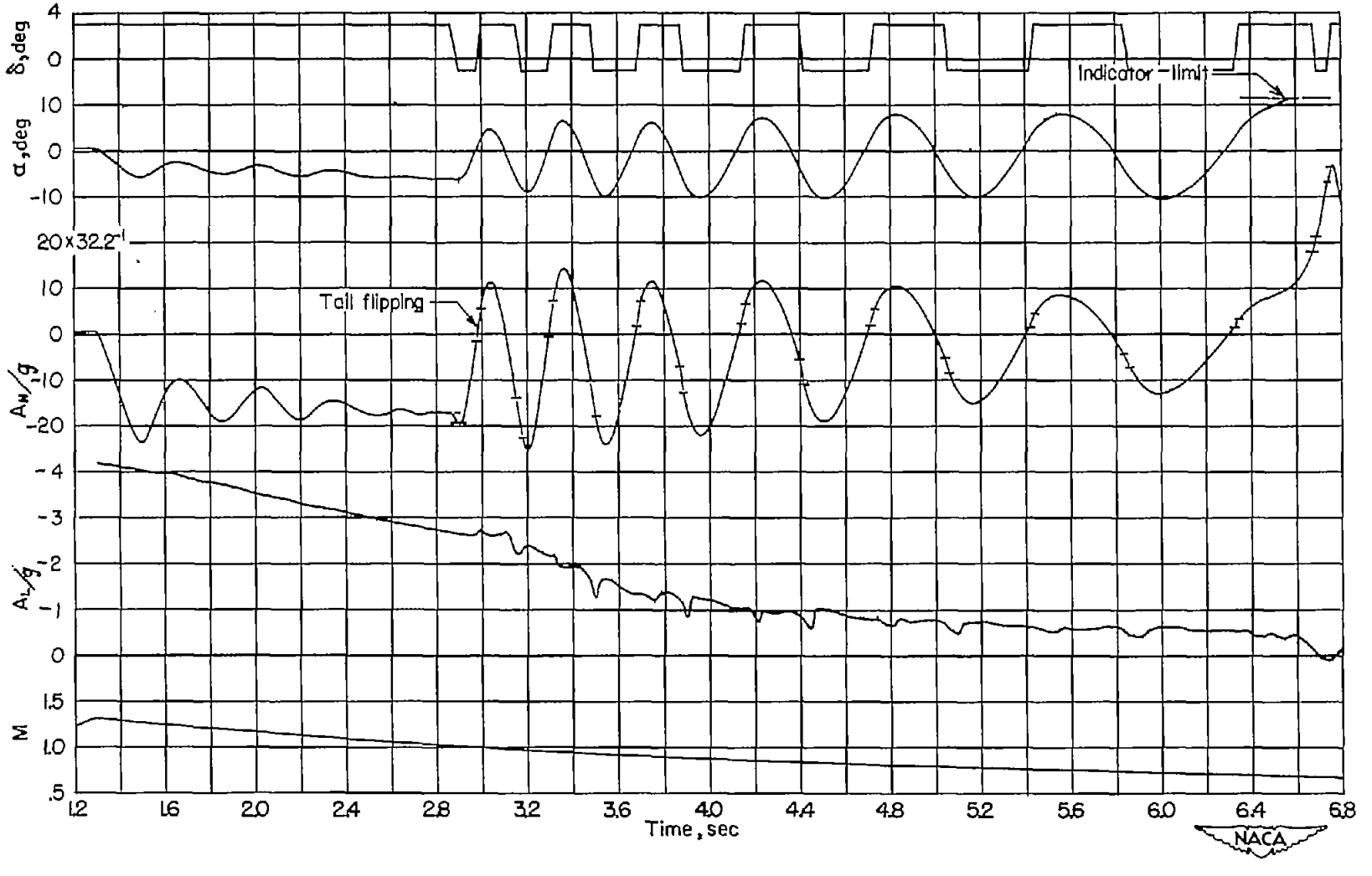

Figure 6.- Time history showing pitching oscillations of model after separation from booster.

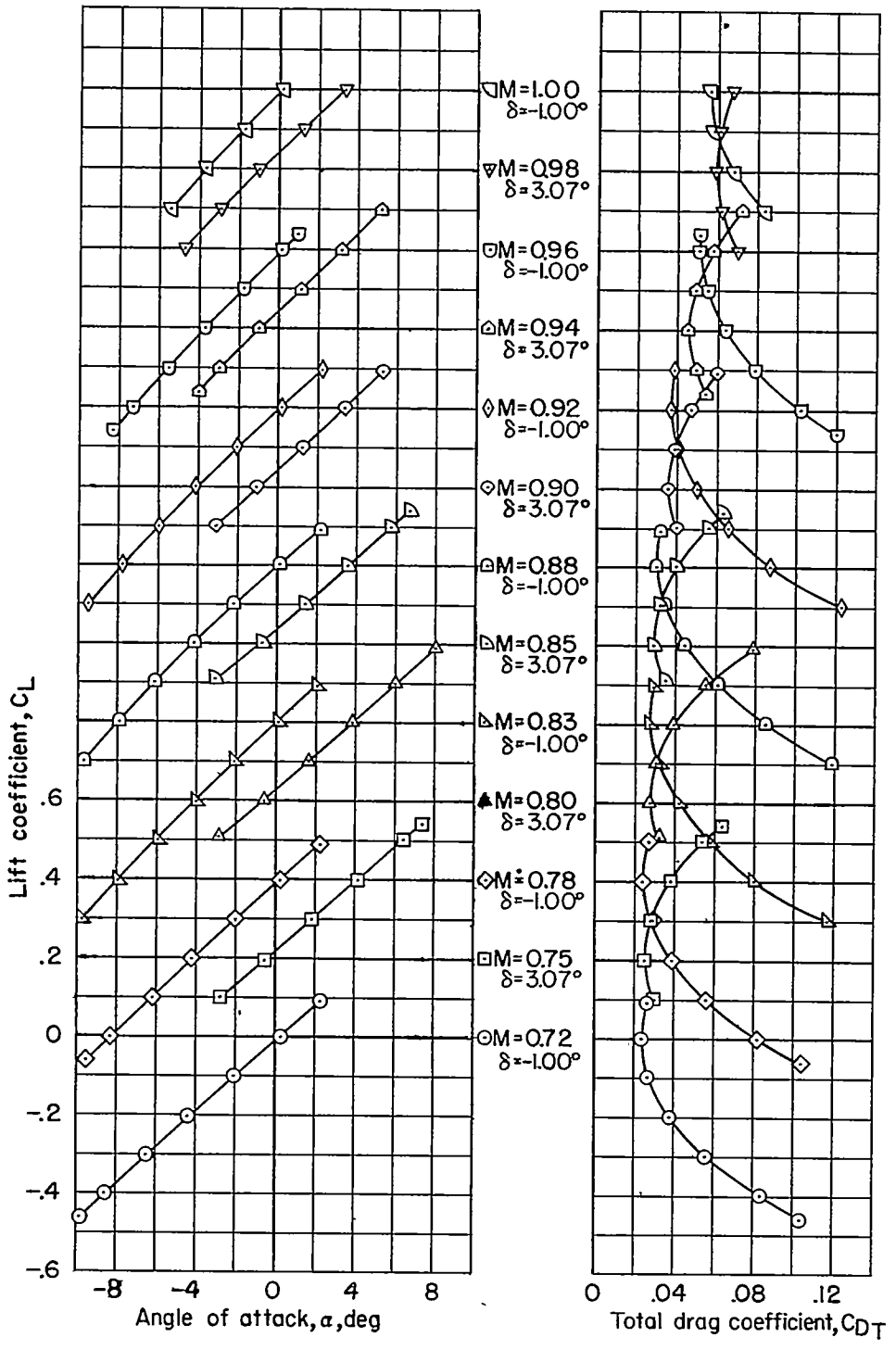

(a) During aeropulsing.

Figure 7.- Lift coefficient plotted against angle of attack and total drag coefficient.

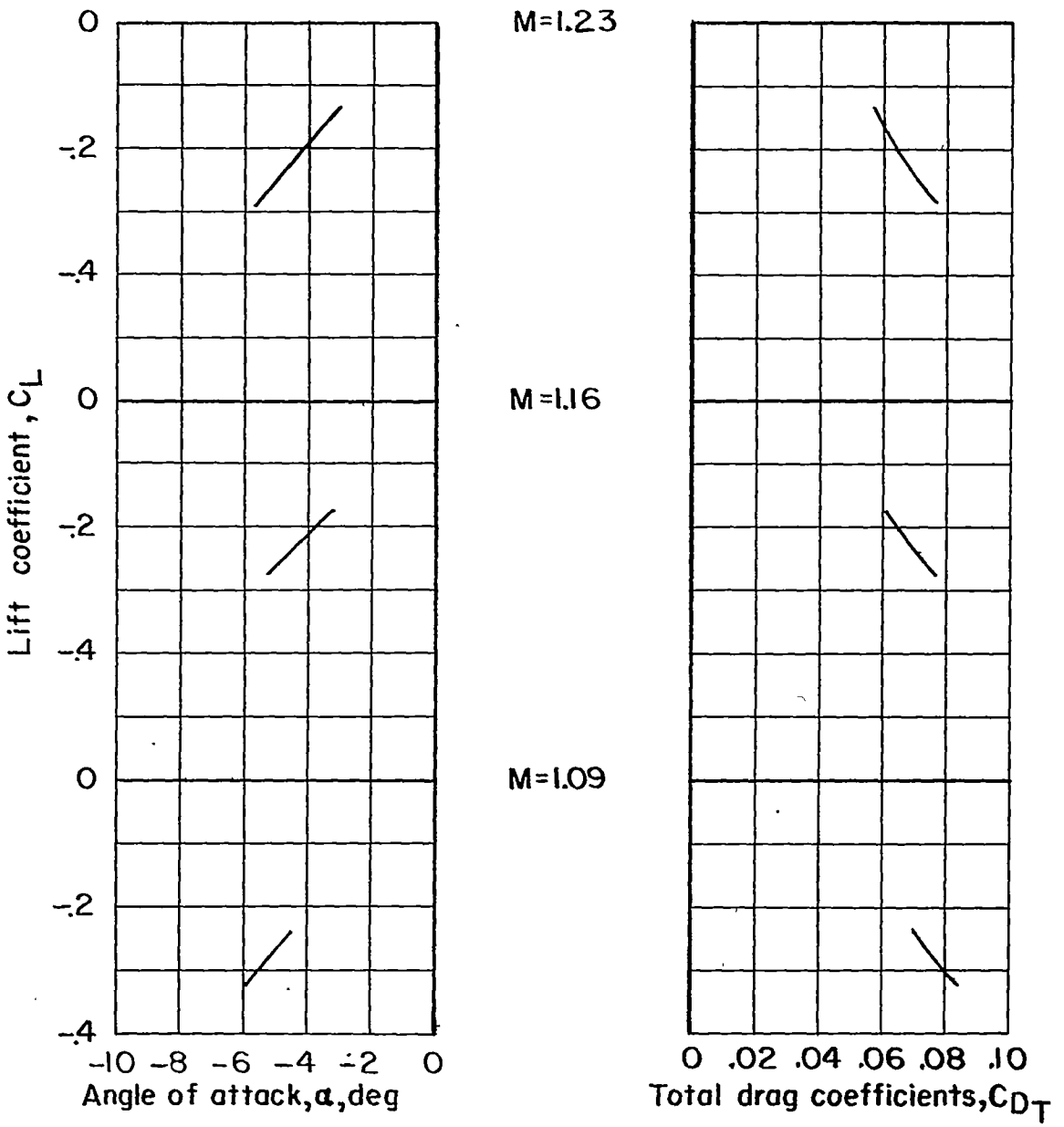

(b) During damped oscillation, $\delta = 3.07^{\circ}$.

Figure 7.- Concluded.

CONFIDENTIAL

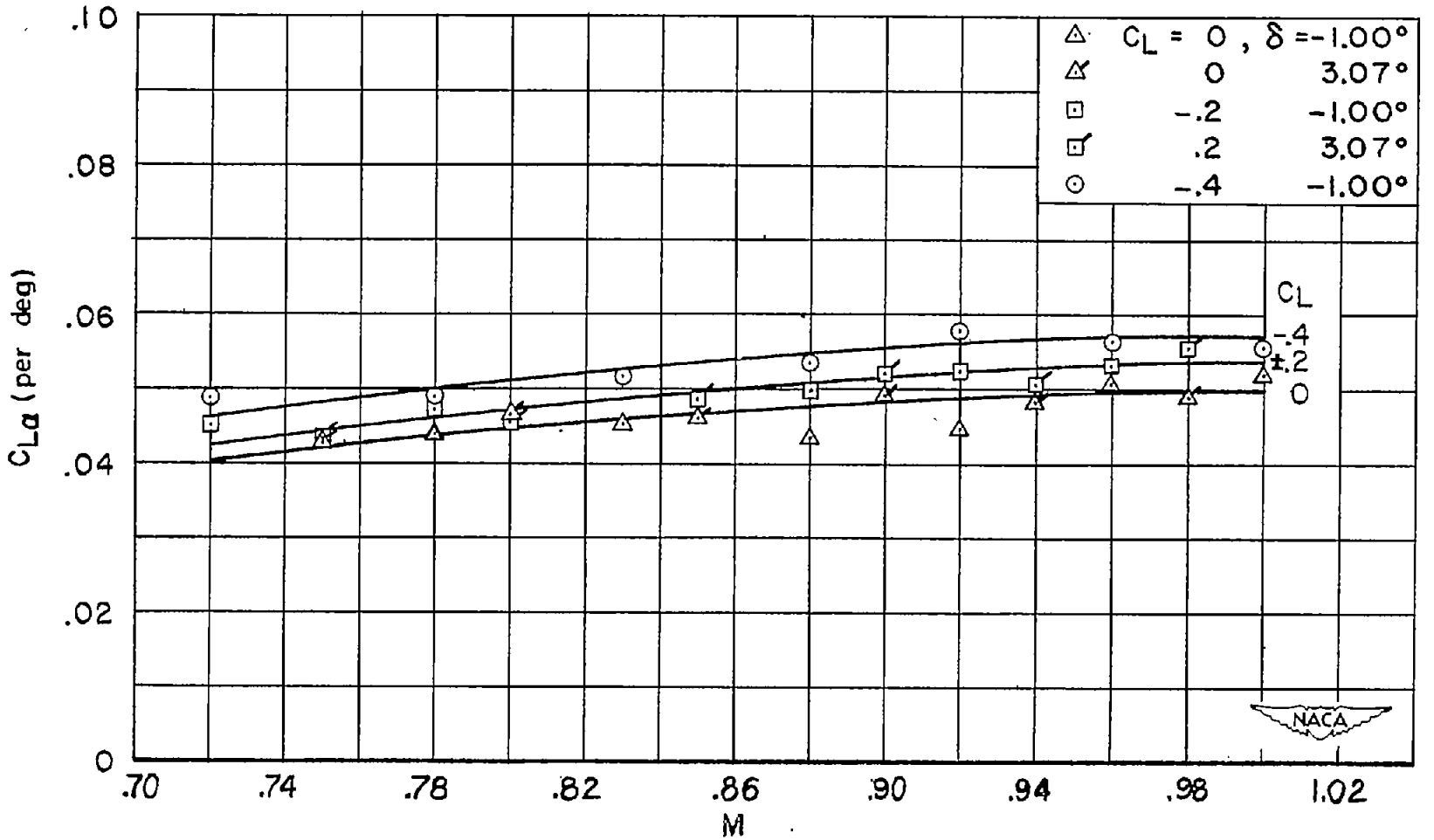

Figure 8.- Lift-curve slope against Mach number.

CONFIDENTIAL

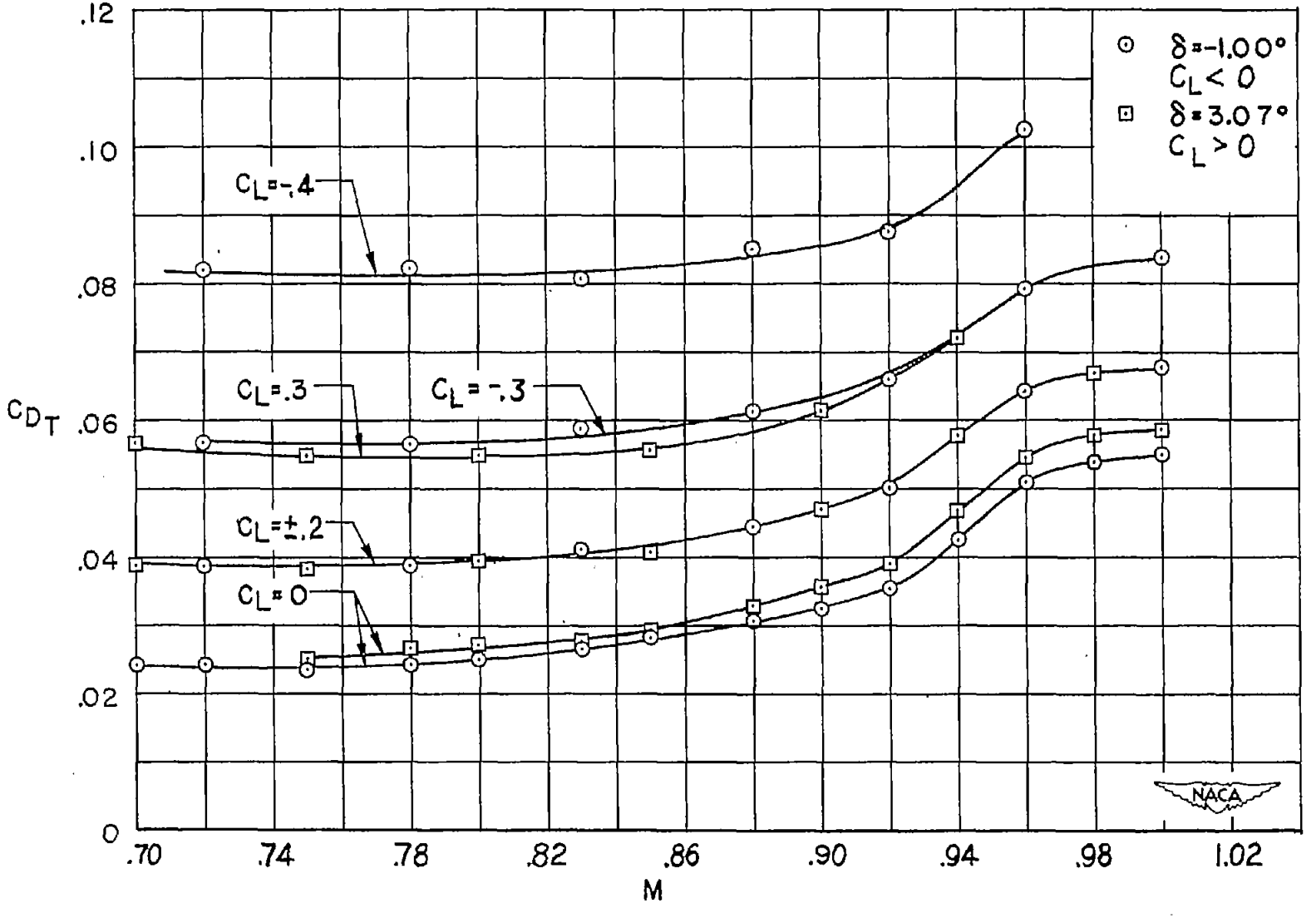

Figure 9.- Total drag coefficient against Mach number.

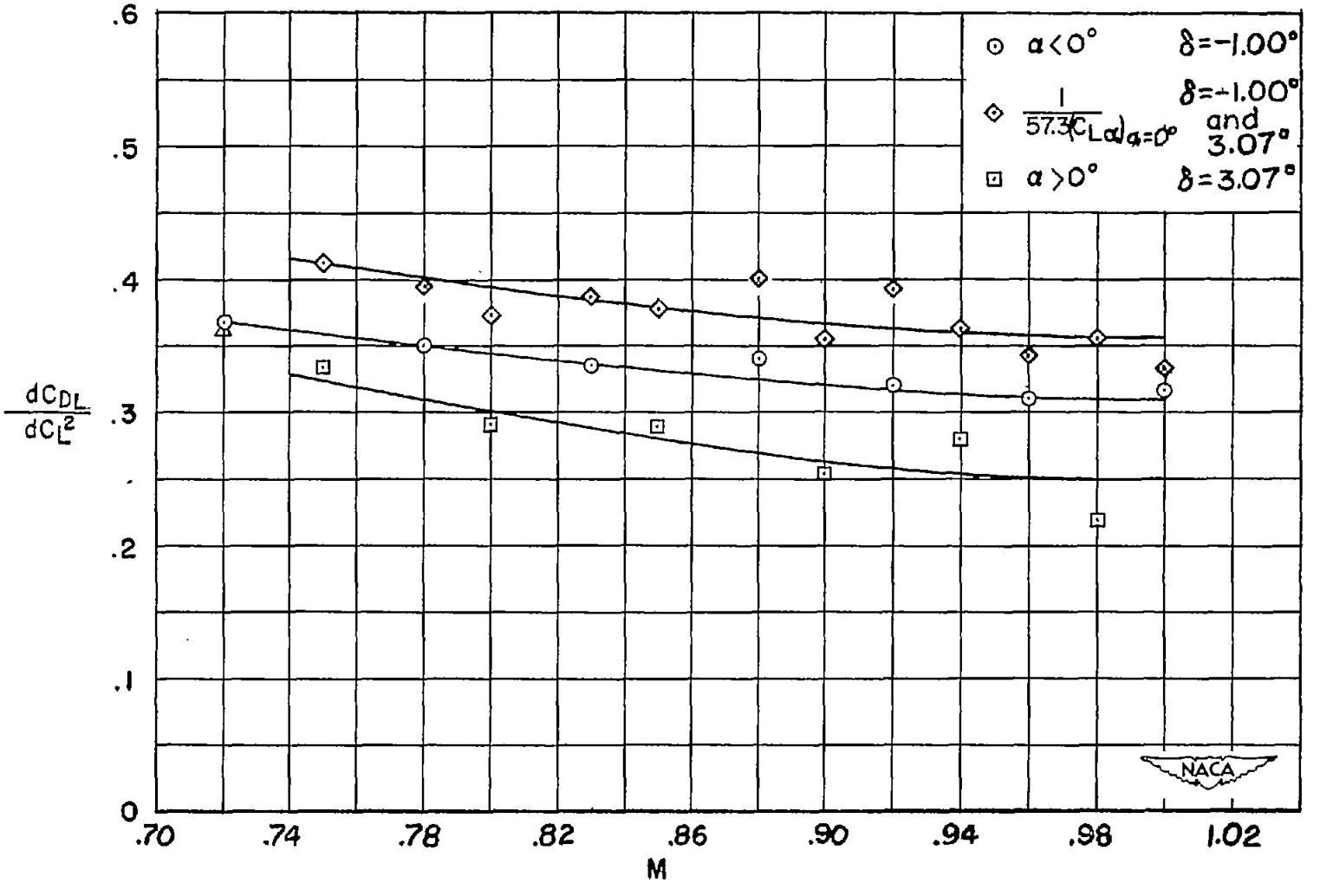

Figure 10.- Drag parameter $\frac{dC_{D_L}}{dC_L^2}$ against Mach number.

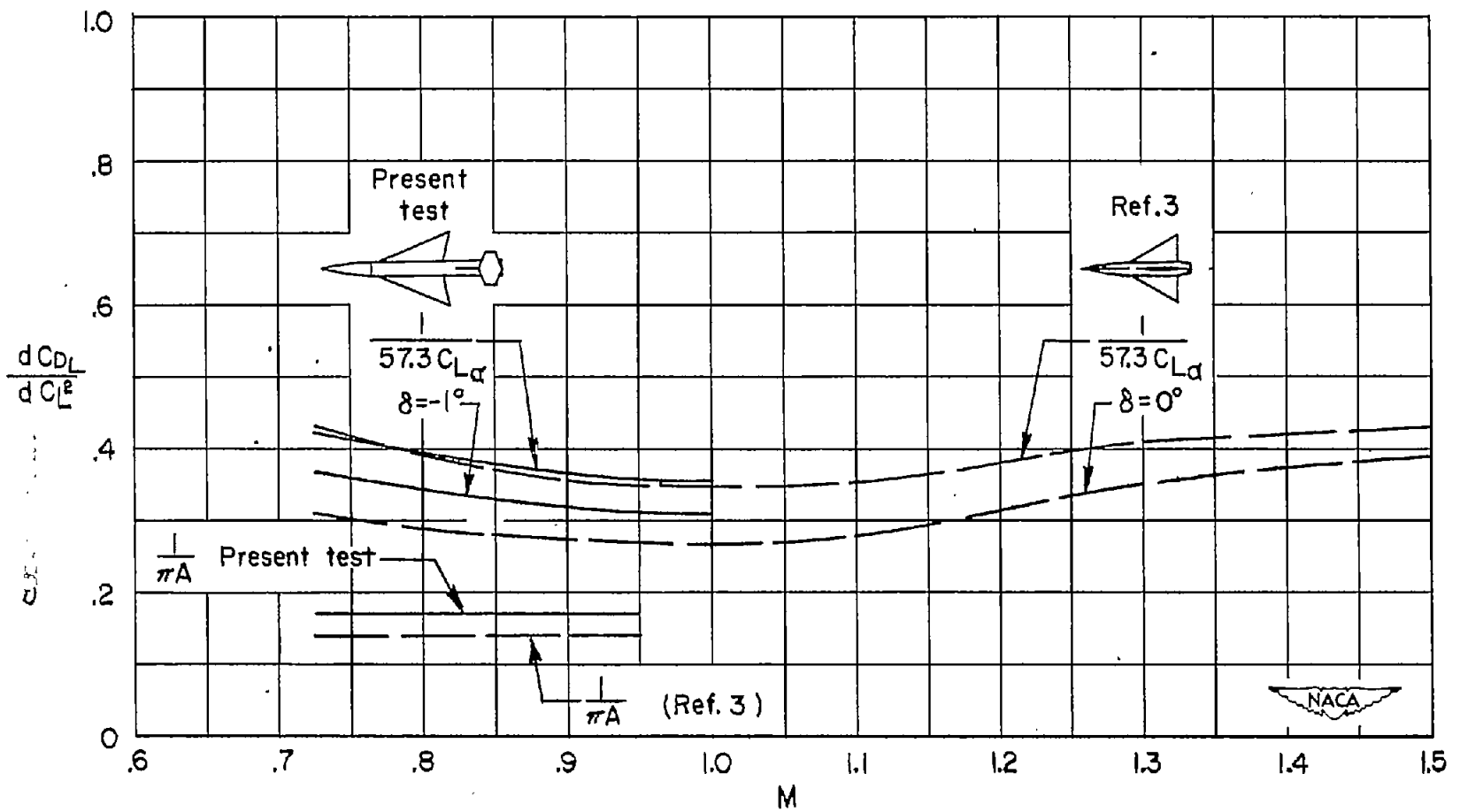

Figure 11.- Comparison of drag parameter $\frac{dC_{D_L}}{dC_L^2}$ for two similar configurations.

[redacted]

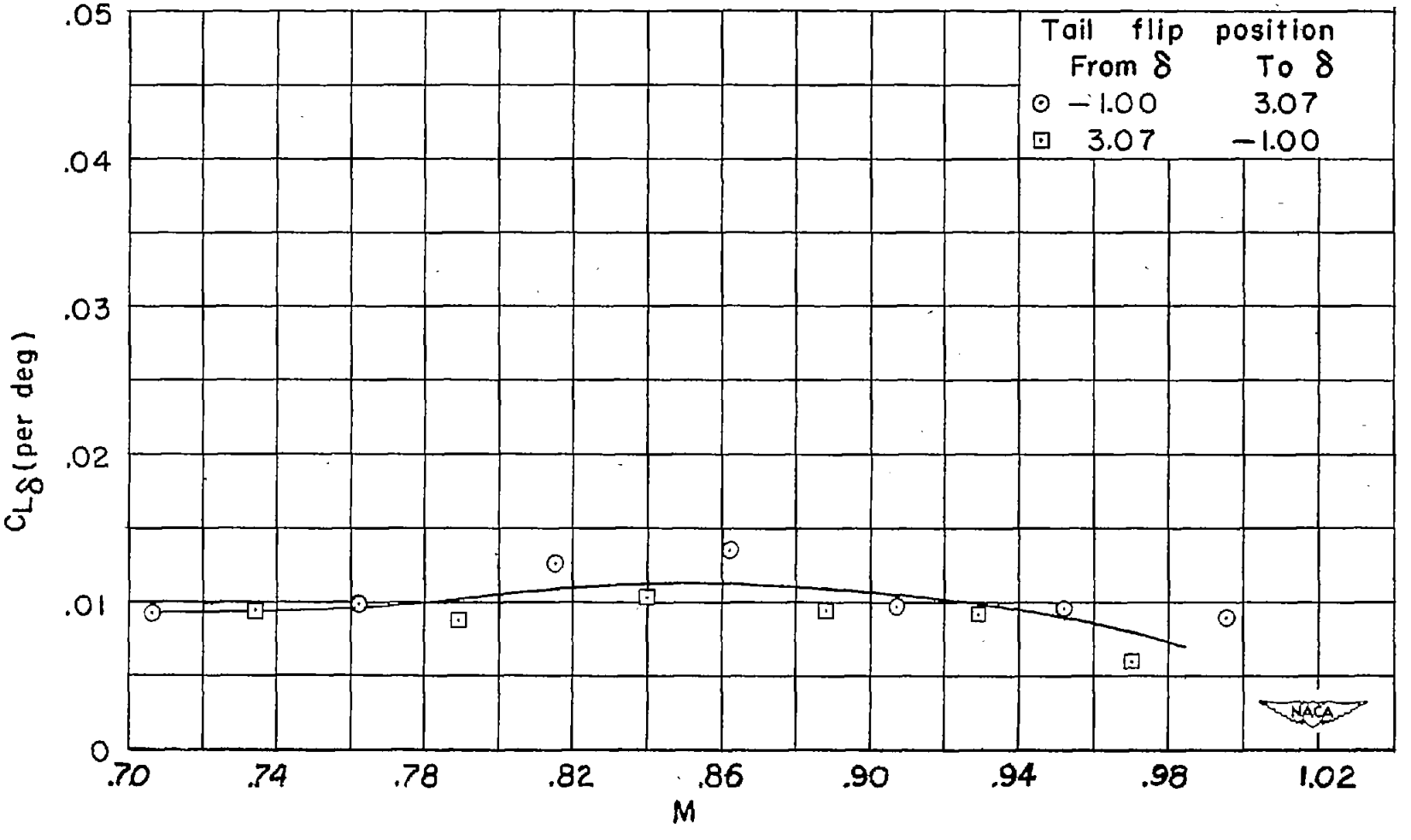

Figure 12.- Lift effectiveness of horizontal tail.

[redacted]

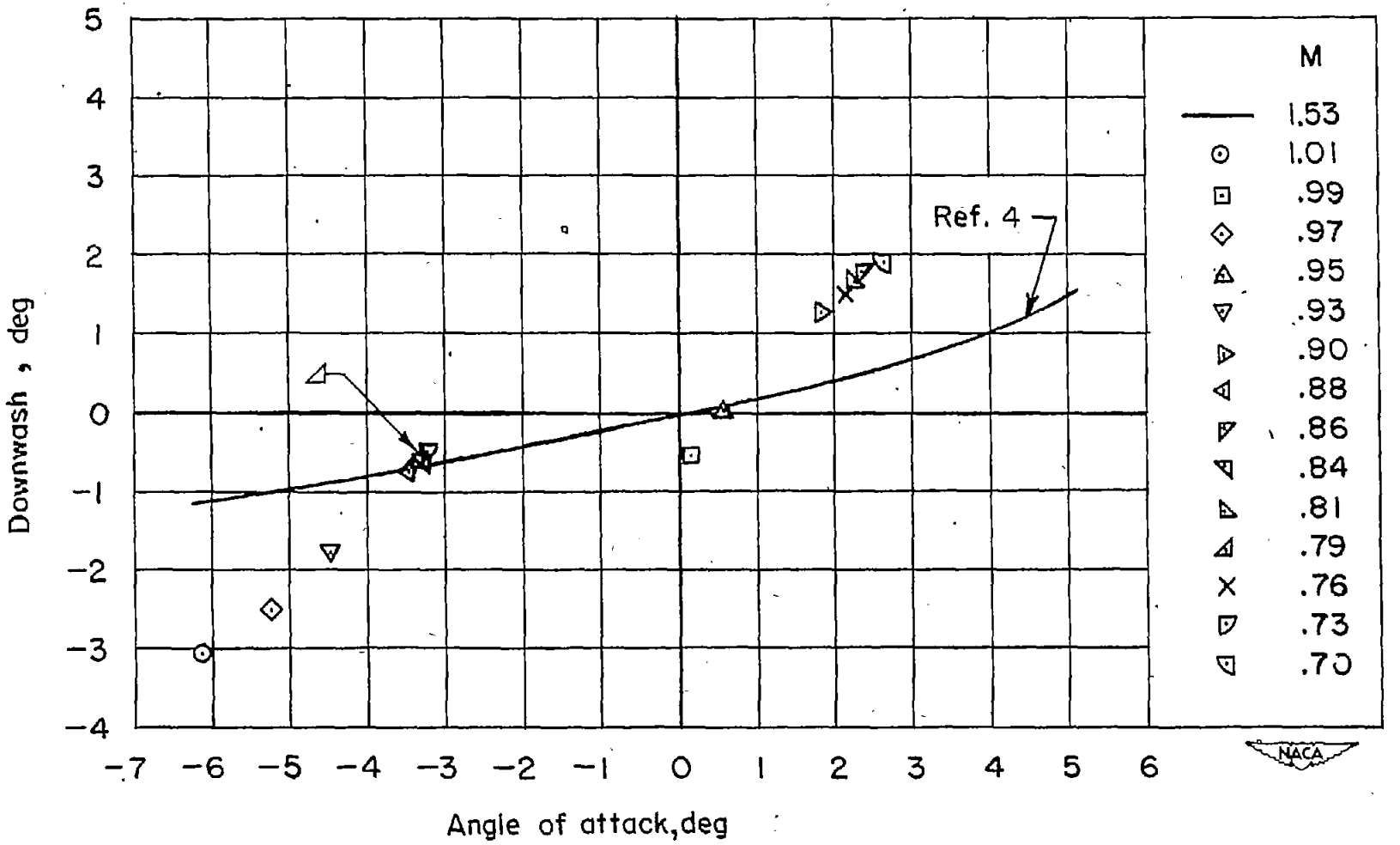

Figure 13.- Effective downwash at horizontal tail.

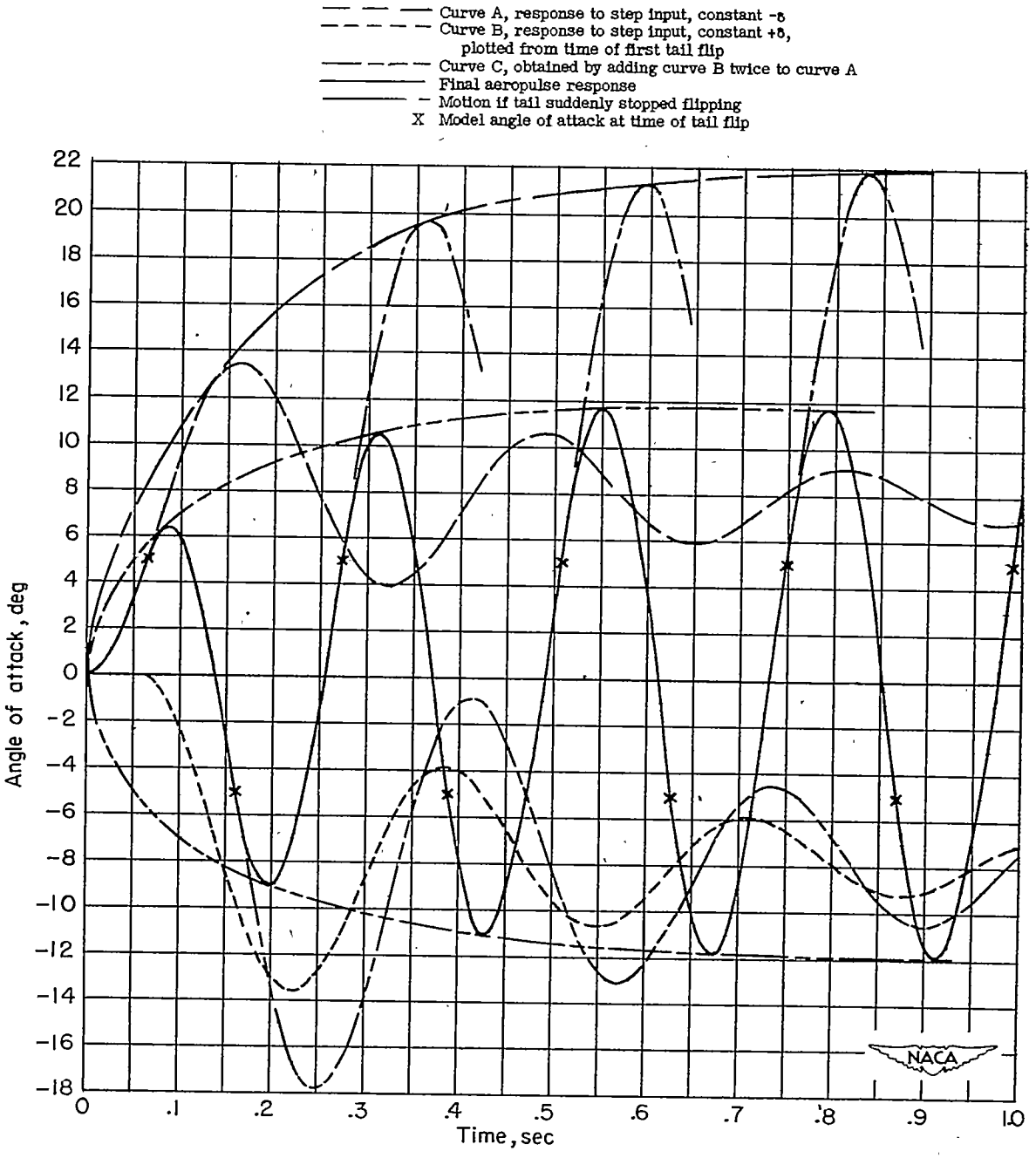

gure 14.- Graphical solution to obtain angle-of-attack response to aeropulsed tail. Mach number, 0.82; center of gravity at 20 percent mean aerodynamic chord; $\delta = \pm 3^{\circ}$; $\frac{d\epsilon}{d\alpha} = 0.40$. Configuration of reference 1.

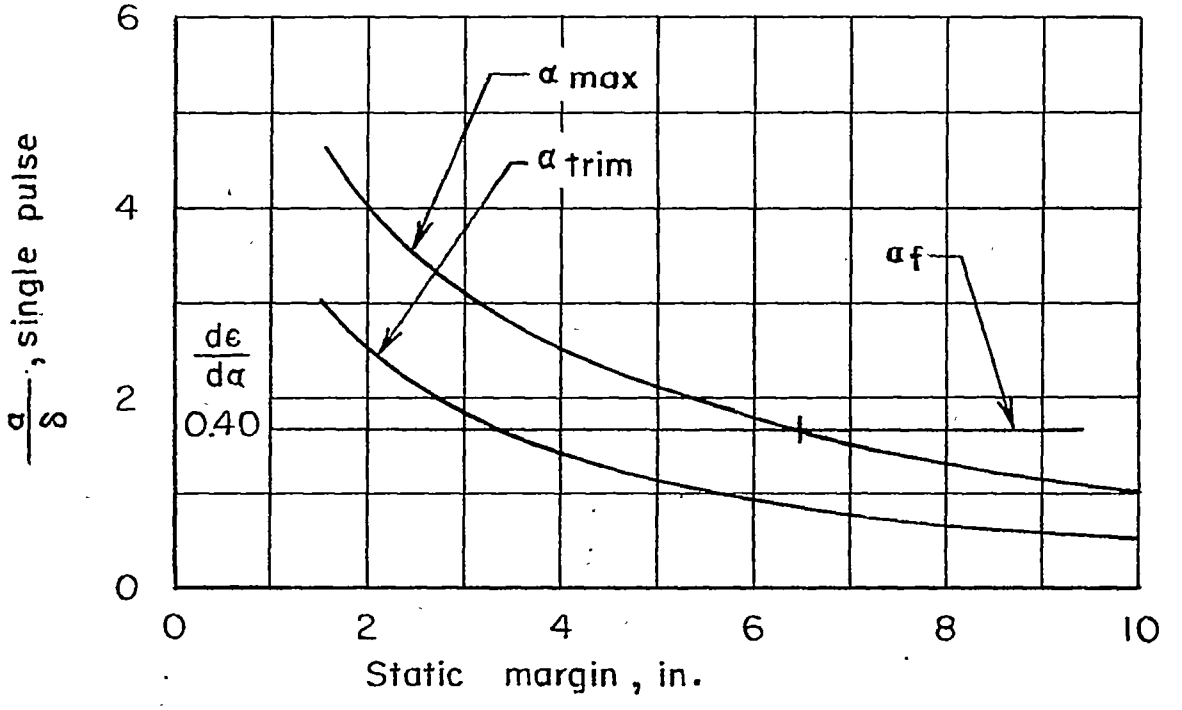

(a) α/δ response to a step input.

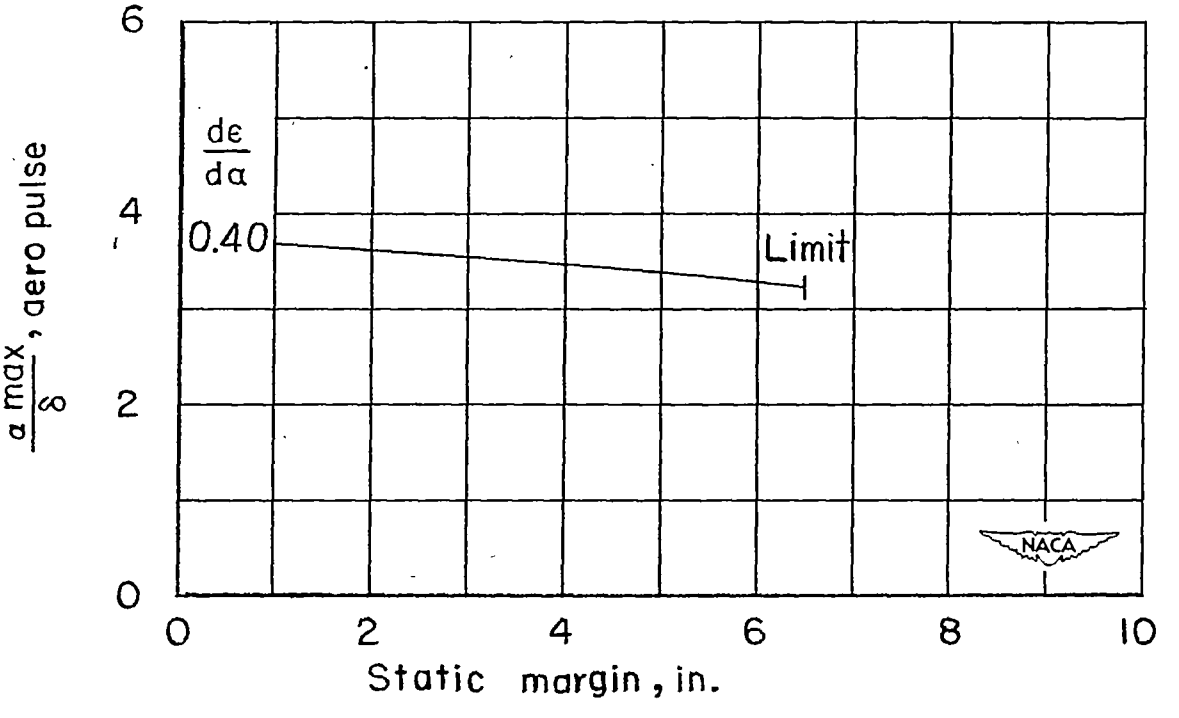

(b) α/δ response to aeropulsing.

Figure 15.- Effect of static margin on response to unit deflection of horizontal tail at Mach number 1.3. Configuration of reference 1.

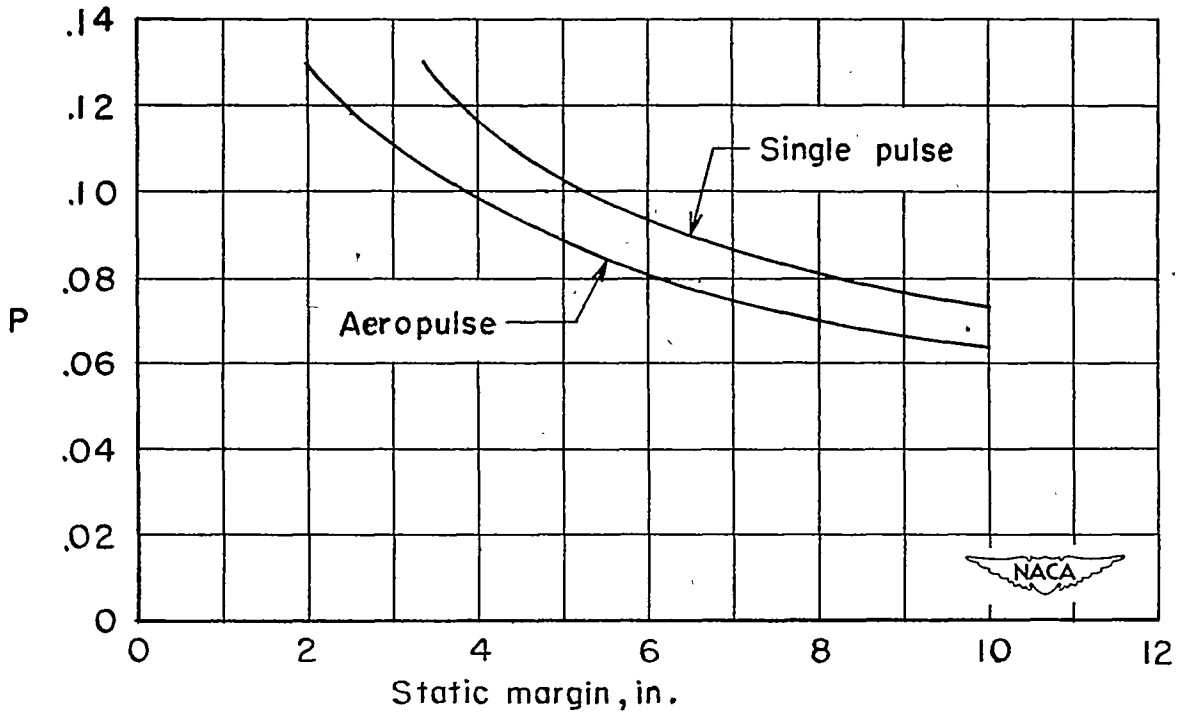

(c) Period with single pulse and aeropulse.

Figure 15.- Concluded.

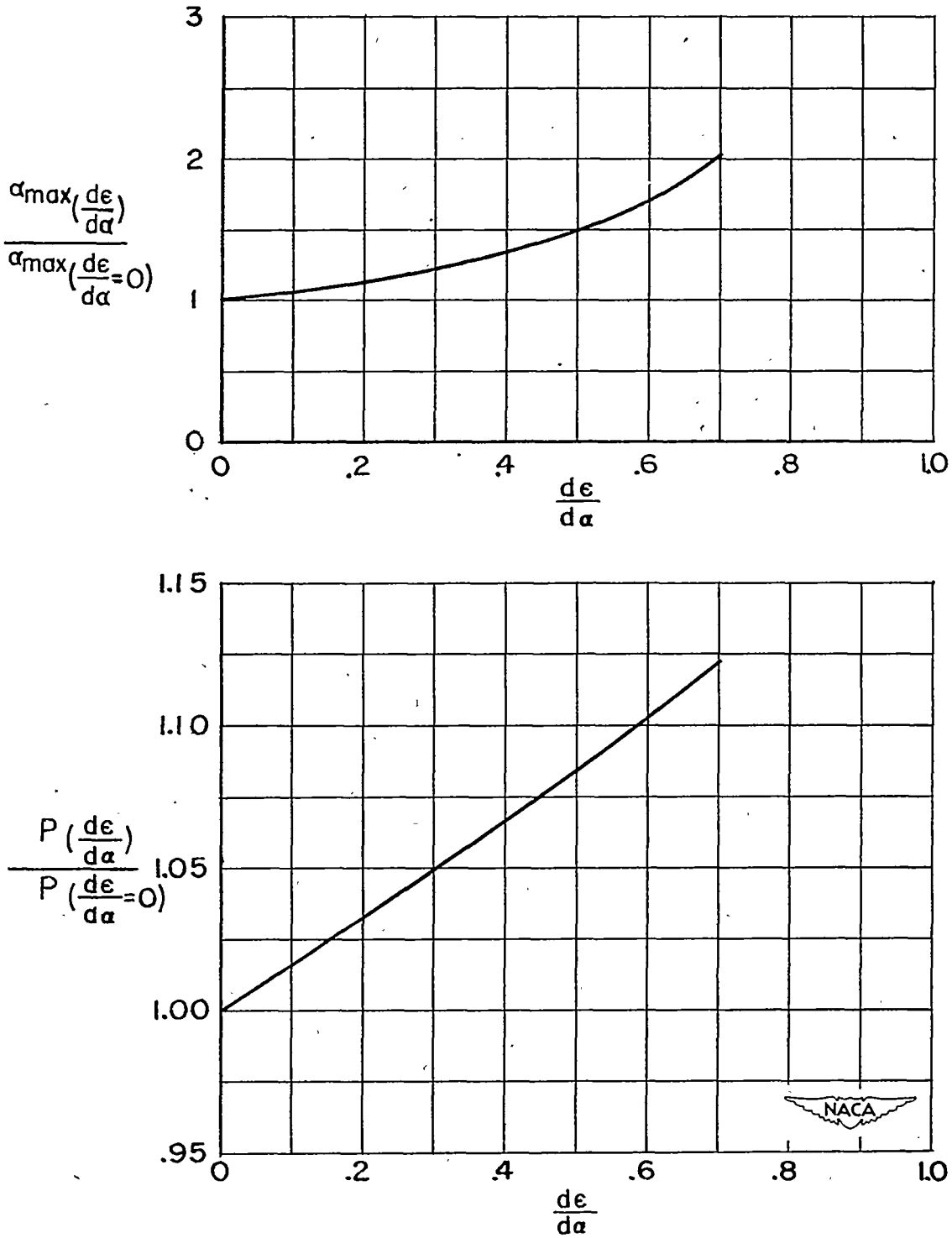

Figure 16.- Variation of α_{max} and period ratios with downwash for aeropulsing. Mach number, 1.3; center of gravity at 20 percent mean aerodynamic chord. Configuration of reference 1.

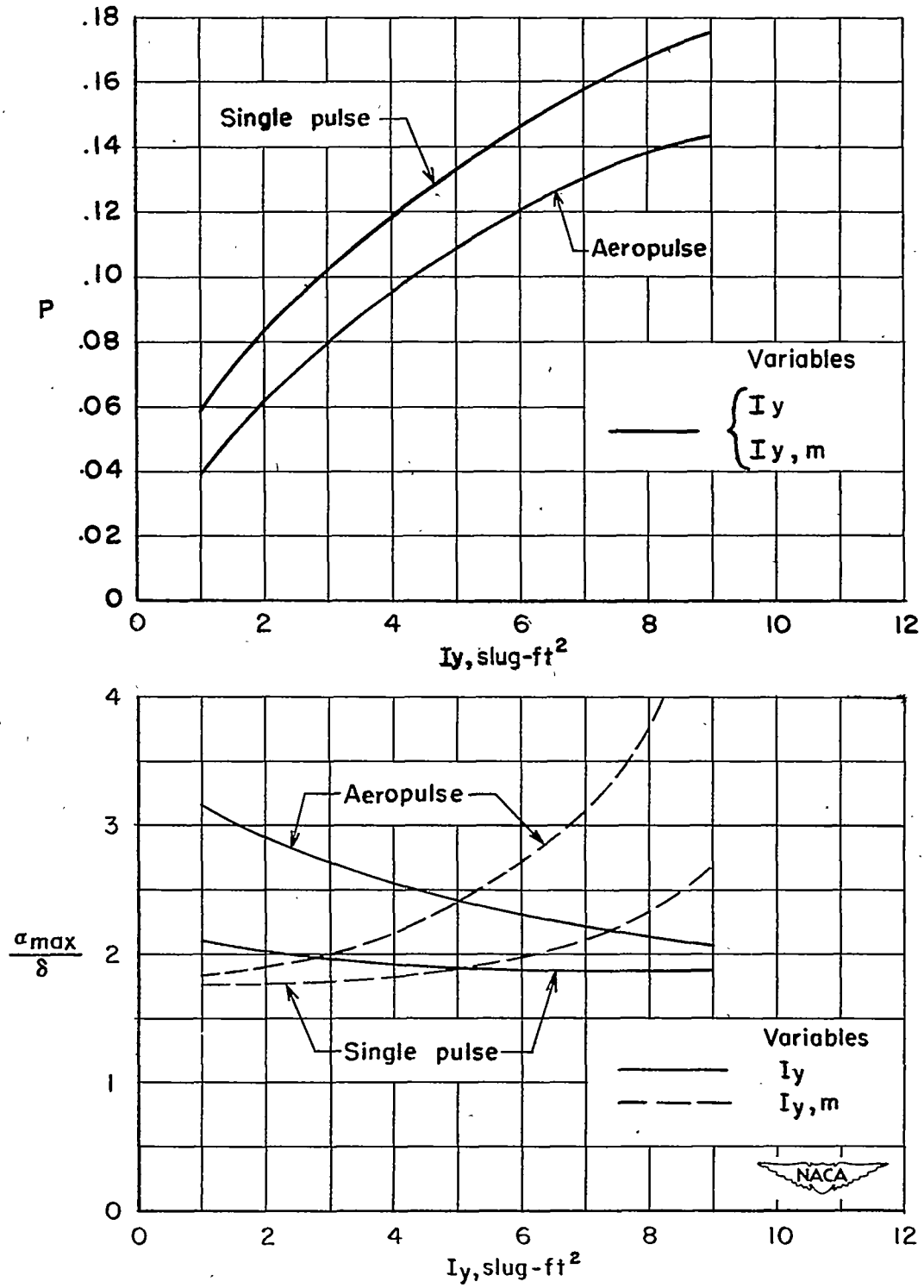

Figure 17.- Variation of α_{max}/δ and period with longitudinal inertia for step input and aeropulsing. Mach number, 1.3; center of gravity at 20 percent mean aerodynamic chord. Configuration of reference 1.

SECURITY INFORMATION

~~CONFIDENTIAL~~

Copy 228
RM L52C10

NACA RM L52C10

TECH LIBRARY KAFB, NM
0143837

NACA

RESEARCH MEMORANDUM

USE OF AN AERODYNAMICALLY PULSED ALL-MOVABLE HORIZONTAL TAIL TO OBTAIN LONGITUDINAL CHARACTERISTICS OF ROCKET-POWERED MODELS IN FREE FLIGHT AND SOME INITIAL RESULTS FROM AN ARROW-WING-BODY-TAIL CONFIGURATION

By Warren Gillespie, Jr. and Albert E. Dietz

Langley Aeronautical Laboratory
Langley Field, Va.

[redacted]

This material contains information affecting the [redacted] of the [redacted], U.S.C., Secs. 793 and 794, the transmission or revelation of which in any [redacted] to an unauthorized person is prohibited by law.

NATIONAL ADVISORY COMMITTEE
FOR AERONAUTICS

WASHINGTON
May 19, 1952

~~CONFIDENTIAL~~

PERMANENT RECORD

Classification cancelled (or changed to Unclassified)

By Authority: NASA Tech Pub Announcement #98
(OFFICER AUTHORIZED TO CHANGE)

By ..... 26 Mar 56

NK

GRADE OF OFFICER MAKING CHANGE)

7 Apr 61
DATE

TECH LIBRARY KAFB, NM
0143839

NATIONAL ADVISORY COMMITTEE FOR AERONAUTICS

RESEARCH MEMORANDUM

USE OF AN AERODYNAMICALLY PULSED ALL-MOVABLE HORIZONTAL TAIL TO OBTAIN LONGITUDINAL CHARACTERISTICS OF ROCKET-POWERED MODELS IN FREE FLIGHT AND SOME INITIAL RESULTS FROM AN ARROW-WING-BODY-TAIL CONFIGURATION

By Warren Gillespie, Jr. and Albert E. Dietz

SUMMARY

The application of an aerodynamically pulsed horizontal tail to determine experimentally the longitudinal aerodynamic characteristics of a rocket-powered model in free flight has been studied. The all-movable horizontal tail was mass-balanced about a hinge line located aft of the tail aerodynamic center. A square-wave pulse was continuously generated when the tail automatically flipped between stop settings.

A graphical procedure for determining the pitching response was applied to an assumed rocket model of a swept-wing airplane configuration to investigate the feasibility of aerodynamic pulsing. Effects of varying the model static margin, downwash at the tail, longitudinal inertia, and inertia and weight together upon the pitching response were investigated.

The technique was then applied experimentally to a rocket-powered model having an arrow wing of 67.5° leading-edge sweep, aspect ratio 1.85, body of fineness ratio 11.1, a ratio of body diameter to wing span of 0.23, and an unswept horizontal tail of aspect ratio 2.3. The Mach number range covered during the time the model continually pulsed was 0.69 to 1.00.

Both preflight calculations and flight-test data showed that downwash from the wing increases the angle of attack at which the tail will flip. The steady-state angle-of-attack response to a unit tail deflection should, therefore, be slightly greater than the required angle of attack to flip the tail in order to insure that a continuous pitching oscillation will develop.

Data were obtained on the drag due to lift, lift-curve slope for the range of lift coefficient 0.2 to -0.4, the tail effectiveness, and downwash at tail flip angles of the test model.

INTRODUCTION

Two types of pulsing methods are currently used to obtain longitudinal aerodynamic characteristics from pitching oscillations of free-flight models. One of these methods employs power-driven mechanisms within the fuselage to drive movable external surfaces which act on the air stream. The other method uses small pulse rockets to disturb the model from trim. The first method limits the space available in the fuselage and places undesirable restrictions on the use of sustainer rocket motors, usually requiring large external booster rockets to attain moderately high Mach numbers. The internal pulsing mechanism is difficult to design, build, and operate. Oscillations obtained by the second method are limited by the number of pulse rockets that can be carried in the model. The time of firing of individual pulse rockets cannot be accurately controlled when delay-squib ignition is used. Data may not be obtained at the Mach number for which data are desired. The oscillations obtained by these two methods generally reduce in amplitude after each pulse so that data at maximum angles of attack are limited to the first oscillation of each pulse. In view of the limitations noted above, a third method has been considered.

The simplified pulsing method reported herein makes use of aerodynamic forces acting on an all-movable horizontal tail. This method has been developed experimentally on a simple rocket-powered model. The horizontal tail is mass-balanced and hinged aft of its aerodynamic center. A continuous pitching oscillation of approximately constant amplitude is sustained throughout the Mach number range as the tail automatically flips between stop settings as the tail lift changes direction. Calculations were first made for an assumed rocket model of the swept-wing airplane configuration of reference 1 for which the static margin, downwash, longitudinal inertia, and inertia and weight together were varied to determine the effect on the pulsing response. These calculations indicated that the method was feasible. An experimental test was conducted using a rocket-powered model having an arrow wing of 67.5° leading-edge sweep, aspect ratio 1.85, body of fineness ratio 11.1, and an unswept horizontal tail of aspect ratio 2.3.

As the model coasted from a Mach number of 1.00 to a Mach number of 0.69, the horizontal tail moved between deflections of -1.00° and 3.07° in approximately a square-wave pattern. The basic aerodynamic parameters of the configuration were determined from the pitching response of the model to the tail motion. The model was flown at the Langley Pilotless Aircraft Research Station, Wallops Island, Va.

SYMBOLS

V	forward velocity, feet per second
q	dynamic pressure, pounds per square foot
g	gravitational acceleration, 32.2 feet per second per second
M	free-stream Mach number
m	model mass, slugs
A	aspect ratio
S	wing area (wing assumed to extend to model center line)
$\bar{c}$	mean aerodynamic chord
α	angle of attack of model, degrees
α_f	angle of attack of model at tail flip, degrees
δ	horizontal-tail deflection, degrees
ϵ	effective downwash angle, degrees
t	time, seconds
I_y	moment of inertia in pitch, slug-feet square
C_L	lift coefficient
C_{L_α}	lift-curve slope for complete configuration
C_{m_α}	moment-curve slope for complete configuration
C_{L_δ}	lift-curve slope for horizontal tail alone
C_{m_δ}	moment-curve slope for horizontal tail alone
C_{D_T}	total drag coefficient
C_{D_L}	drag due to lift
C_{m_q}, $C_{m_{\dot{\alpha}}}$	model damping coefficients

A_N normal acceleration, feet per second per second

A_L longitudinal acceleration, feet per second per second

P period, seconds

X distance from the model center of gravity to the aerodynamic center of the horizontal tail, feet

The coefficients are based on wing area.

MODEL AND TEST

Figure 1 shows the geometric details of the rocket-powered flight-test configuration. Figure 2 presents photographs of the free-flight model; figure 3 shows close-up views of the horizontal tail surface and empennage; and figure 4 shows the model-booster combination in launching position. The model was made of magnesium alloy with the exception of the horizontal tail which was made of steel. The tail pivot support was enclosed by a fairing. Stops for the horizontal tail were mounted on the tip of the vertical tail. The tail was free to flip between stop settings of -1.00° and 3.07°. The model was instrumented with a four-channel telemeter which transmitted continuous records of angle of attack, total pressure, and normal and longitudinal acceleration. Horizontal-tail position was indicated by the total-pressure trace which shifted electrically a constant known amount when the tail moved from one stop position to the other.

The model was propelled to maximum speed by means of a booster. At booster burnout the model separated from the booster and coasted through the test Mach number range of approximately 1.30 to 0.69 which corresponds to a Reynolds number range (fig. 5) of approximately 13.5×10^6 to 6.3×10^6, respectively. Time histories of normal and longitudinal accelerations, total pressure, and angle of attack were obtained by standard NACA procedures, reference 2, and used in conjunction with velocity and position tracking radar and radiosonde measurements to permit evaluation of aerodynamic quantities as a function of Mach number.

TECHNIQUE

This pulse method employs a tail surface that is mass-balanced and free to rotate about an axis located aft of the tail aerodynamic-center position. The maximum rotation of the surface in either direction is

limited by a stop. Lift on the tail surface holds the surface against a stop until the pitching motion of the model induced by the tail lift reverses the lift on the tail. The tail then flips suddenly against the other stop to reverse the pitching motion. As the angle of attack builds up in the other direction, the tail flips back to the first stop position. This action continues automatically as the model coasts. The model angle of attack at which the tail should flip is a function of the effective downwash over the horizontal tail at the time of flip, the tail-wing setting before flip, and the pitching-velocity contribution to the tail angle of attack at the time of flip. Since the tail is moved by aerodynamic forces, this pulsing technique will be referred to as the "aeropulse" technique.

The aeropulse technique was applied to an assumed model of the swept-wing airplane configuration of reference 1 to check the feasibility of obtaining longitudinal aerodynamic characteristics of tail-last configurations. The results of this general analysis are presented in appendix A.

The technique was then applied to the free-flight rocket-powered model of figure 1 which was successfully flight-tested. Methods used in obtaining the longitudinal characteristics of aeropulsed models from experimental free-flight data are presented in appendix B.

ACCURACY

The limitations of the technique used are discussed in reference 2. For the flight model of the present paper, the maximum possible errors in the absolute values of Mach number, angle of attack, C_L, and C_D have been estimated. It should be emphasized that the probable error may be much less than the values presented in the following table:

	M = 1.00	M = 0.70
ΔM	±0.02	±0.02
$\Delta\alpha$, degrees	±0.50	±0.50
ΔC_L	±0.026	±0.060
ΔC_D	$\pm(0.0034 + 0.026 \sin \alpha)$	$\pm(0.0079 + 0.060 \sin \alpha)$

FREE-FLIGHT MODEL RESULTS AND DISCUSSION

Time History

A time history of the coasting portion of flight, figure 6, presents the variation of tail position, angle of attack, normal and longitudinal accelerations, and Mach number. The model separated from its booster at approximately 1.30 seconds from take-off and responded to the 3.07° tail deflection. The model did not begin immediate pulsing since the angle-of-attack response was insufficient to force the tail to flip to the opposite -1.00° stop setting. The oscillation induced by separation of the model from its booster damped as the model trim angle increased negatively with reduced Mach number.

At a trim angle of -6.1° and Mach number 1.01 the tail flipped and the automatic pitching oscillation developed. Between Mach numbers 1.01 and 0.69 a continuous square-wave pulse was generated by the tail. At the lower Mach number of 0.69 the model became unstable. The static margin was very small at this Mach number and the angle-of-attack limit for static stability was reached at the peak of the cycle.

Lift and Drag

Figure 7 presents lift coefficient plotted against angle of attack and drag coefficient at constant Mach numbers and tail settings. Figure 7(a) presents data during the aeropulsing portion of flight for both tail positions, and figure 7(b) presents data from the damped oscillation for the 3.07° tail setting.

Figure 8 shows the variation of model lift-curve slope with Mach number at constant C_L values of 0, ±0.2, and -0.4. Both increasing Mach number and increasing C_L caused an increase in C_{L_α}.

Figure 9 presents the variation of total drag coefficient with Mach number at constant lift coefficients of 0, ±0.2, and ±0.3 for both tail settings and at a lift coefficient of -0.4 for the -1.00° tail setting. The curves show a gradual drag rise starting at a Mach number of approximately 0.8.

Figure 10 presents the variation of drag due to lift with Mach number for the cases when $\alpha < 0^{\circ}$, $\delta = -1.00^{\circ}$; $\alpha > 0^{\circ}$, $\delta = 3.07^{\circ}$; and $1/57.3C_{L_\alpha}$ at $\alpha = 0^{\circ}$, $\delta = 3.07^{\circ}$ and -1.00°. Figure 11 shows that the drag due to lift for the model tested is greater than the drag due to lift for the 60° delta wing-body configuration of reference 3, which had an NACA $65_{(06)}$A006.5 airfoil section. The model of the present test

had a flat-plate wing with a pointed leading-edge section and may have experienced greater leading-edge separation than the model of reference 3. The drag due to lift is more closely approximated at subsonic speeds by the parameter $1/57.3C_{L_\alpha}$ than by $1/\pi A$ although both are presented for comparison.

Tail Effectiveness and Downwash

Figure 12 shows the variation of tail-lift effectiveness with Mach number obtained from changes in tail position which occurred at low lifting conditions. The tail effectiveness coefficient varied slightly about an average 0.01 value throughout the test range.

The effective downwash values at the tail are presented in figure 13 for the Mach numbers occurring at the time of tail flips and are plotted against the angles of attack of the wing at the time when the downwash was assumed to have been generated. The horizontal tail was displaced above the model center line. For this tail position the downwash was higher at positive angles of attack than at negative angles of attack. Downwash obtained behind a 60° delta wing at Mach number 1.53 and presented in reference 4 indicated similar results due to an elevated tail position.

CONCLUDING REMARKS

An investigation has been made of a simple aerodynamic pulsing system using an all-movable horizontal tail to obtain longitudinal aerodynamic characteristics of a rocket model in free flight. Flight test of a model having an arrow wing of 67.5° leading-edge sweep and aspect ratio 1.85 showed that, with a small amount of static margin and the tail mounted above the fuselage, a continuous pitching oscillation was sustained over an approximately constant angle-of-attack range. Reduction of data permitted an evaluation of model lift and drag, lift-curve slope, drag due to lift, tail effectiveness, and effective downwash at the tail.

Langley Aeronautical Laboratory
National Advisory Committee for Aeronautics
Langley Field, Va.

APPENDIX A

ANALYSIS OF AN ASSUMED MODEL

The longitudinal response to an aerodynamically pulsed tail surface for an assumed rocket model of the sweptback-wing airplane configuration of reference 1 was investigated by a graphical procedure. Basic aerodynamic data required in the analysis were estimated from theory and available experimental data from this and similar configurations.

Figure 14 illustrates the graphical method applied to the assumed model with center of gravity at 20 percent mean aerodynamic chord, $d\epsilon/d\alpha$ assumed equal to 0.40, tail stop limits of $\pm 3^{\circ}$, and Mach number of 0.82. The basic response to a step input of -3° tail deflection, curve A of figure 14, was first plotted. Starting at the first angle of attack at which the tail should flip, 5.0° at time equal 0.065 second, the opposite response to a step input of 3° tail deflection, curve B, was plotted. In order to cancel the -3° tail deflection after 0.065 second time and put in the response to the 3° tail deflection, curve B was added twice to the previous curve A. The response curve due to the first tail flip from -3° to 3°, curve C, was therefore obtained. At each subsequent angle of flip, this procedure was repeated; that is, the response curve to a step input, starting from the time of tail flip, was added twice to the previous resulting curve. It should be noted that all the curves must be plotted out to the same time value, otherwise the solution cannot progress. The solution should be continued until the envelopes of the final aeropulse curve approach a constant maximum amplitude. This may occur within three or four oscillations of the basic response curve A.

The aeropulse response can be obtained with better accuracy by using the following analytical solution for a step input with initial conditions taken at the model starting condition and at the time of each succeeding tail flip:

$$\alpha = \alpha_{trim} - \left(\alpha_{trim} - \alpha_o\right)e^{-bt}\left(\frac{b}{a}\sin at + \cos at\right) + \dot{\alpha}_o e^{-bt}\sin at$$

where

$$\alpha_{trim} = -\frac{\frac{mV}{57.3qS}C_{m_\delta}\delta + C_{L_\delta}\delta\, C_{m_q}\frac{\bar{c}}{2V}}{\frac{mV}{57.3qS}C_{m_\alpha} + C_{L_\alpha}C_{m_q}\frac{\bar{c}}{2V}}$$

$$b = \frac{57.3qS}{2}\left[\frac{C_{L_\alpha}}{mV} - \frac{\left(C_{m_q} + C_{m_{\dot{\alpha}}}\right)\bar{c}^2}{2VI_y}\right]$$

$$a = \left[-\frac{57.3qS}{I_y}\left(C_{m_\alpha}\bar{c} + \frac{C_{L_\alpha}C_{m_q}\ 57.3qS\bar{c}^2}{2mV^2}\right) - b^2\right]^{1/2}$$

and α_o and $\dot{\alpha}_o$ are the initial angle of attack and the angular velocity, respectively.

The effects of varying the model center-of-gravity position, downwash at the tail, longitudinal inertia, and inertia and weight together were calculated at Mach number 1.30. Figure 15 shows the effect static margin has upon the single-step and aeropulse responses. The maximum and steady-state α/δ values of figure 15(a) approach infinity as the static margin decreases to zero. The intersection of the horizontal flip-angle line with the maximum α/δ curve defines the maximum allowable static margin that will permit the continuous motion to start from rest, that is, for the particular downwash value assumed. Reference 1 indicated a value of $\frac{d\epsilon}{d\alpha}$ between 0.4 and 0.5 at Mach number 1.30; hence, the static margin for the assumed model under consideration should not be greater than approximately 5 inches at this Mach number. Figure 15(b) shows that the aeropulse system for a constant value of $\frac{d\epsilon}{d\alpha}$ equal to 0.40 should maintain a maximum angle-of-attack response which increases slightly as the static margin decreases from the limiting static margin toward zero. The period of the continuous motion is presented in figure 15(c) and is somewhat less than the natural free period of the model and increases with reduced static margin. Figure 16 shows the effect that downwash at the tail has upon the amplitude of the pitching oscillation and the period. Both the amplitude and period increase with increased downwash. Figure 17 shows the effect longitudinal inertia has upon the period and maximum α/δ for the single pulse and aeropulse when the longitudinal inertia only is varied by distributing the model mass at varying distances from a fixed center-of-gravity position and when the longitudinal inertia is varied by adding and substracting mass at equal distances from a fixed center-of-gravity position. The model was assumed to have an initial moment of inertia of 5.00 slug-feet^2. No difference in period was obtained at a given value of inertia when the mass was changed. Both curves decreased as the inertia approached zero. Unlike the period, there was considerable difference in amplitude

of the maximum values of α/δ for the single pulse and aeropulse for these two conditions. When inertia only was varied, maximum α/δ increased as inertia decreased, but a reverse trend occurred when both inertia and mass were varied together.

The larger peak angle that would result if the tail suddenly stopped flipping (see fig. 14) indicates that, once the aeropulse motion has begun, the motion will probably continue even if the actual downwash at a later time during coasting flight of a model exceeds the downwash that existed at the time the aeropulse motion began. For the assumed model under consideration, the maximum allowable downwash to start the oscillation from rest is greater at subsonic speed than at supersonic speed for the same center-of-gravity position. This condition occurs because the static margin at subsonic speed is less and the response to a unit tail deflection is greater. Application of this pulsing method to a given configuration, therefore, depends largely on the selection of a model center-of-gravity position that will permit the aeropulse motion to start automatically. If the requirements for automatic starting cannot be met by preflight adjustments to the model, use of a small pulse rocket is suggested to disturb the model initially and permit the aeropulse motion to develop.

APPENDIX B

DATA REDUCTION OF THE FLIGHT MODEL

Lift and Drag

The lift and drag coefficients were determined by transferring the normal and longitudinal accelerations measured along the body axes to the stability axes. The angle between the two sets of axes was the model angle of attack. A cross-plotting technique was used over the aeropulse region of Mach number to obtain C_{D_T} and α values at a constant C_L and Mach number. A plot of the time histories of C_L, C_{D_T}, α, and M was made on the same sheet of graph paper; constant C_L values were selected and corresponding points were projected at the same time on the C_{D_T} and α curves. The projected values at constant C_L for each item were then joined by a smooth curve throughout the time-history plot. Lines of selected constant Mach numbers were drawn perpendicular to the time axis through the C_{D_T}, and α curves determined by the projected points. Intersections of these Mach number lines and the lines of C_{D_T} and α corresponding to constant values of C_L resulted in sets of data at constant Mach numbers over the aeropulse region of Mach number. For the Mach number region of the damped oscillation, this cross-plotting technique could not be used. Plots of C_L against α and C_{D_T} were made using the method of reference 2.

Tail Effectiveness and Downwash

The tail lift effectiveness C_{L_δ} was obtained by determining the incremental shift that occurred in the normal-force-time curve (see fig. 6) each time the tail flipped. The normal-force-time curve was extrapolated to the middle of the time interval during tail flipping. This interval was very short, 0.03 second in most cases.

Effective downwash at the horizontal tail surface was determined at the start of each tail flip when the lift on the tail was assumed to be zero. The following equation was used to evaluate the downwash:

$$\epsilon = \alpha + \delta + \frac{X}{V}\left(\dot{\alpha} + 57.3\,\frac{A_N}{V}\right)$$

The downwash was assumed to originate from the wing at an earlier time, $t - \frac{X}{V}$.

REFERENCES

1. Osborne, Robert S.: High-Speed Wind-Tunnel Investigation of the Longitudinal Stability and Control Characteristics of a $\frac{1}{16}$-Scale Model of the D-558-2 Research Airplane at High Subsonic Mach Numbers and at a Mach Number of 1.2. NACA RM L9C04, 1949.

2. Gillis, Clarence L., Peck, Robert F., and Vitale, A. James: Preliminary Results from a Free-Flight Investigation at Transonic and Supersonic Speeds of the Longitudinal Stability and Control Characteristics of an Airplane Configuration with a Thin Straight Wing of Aspect Ratio 3. NACA RM L9K25a, 1950.

3. Mitcham, Grady L., Crabill, Norman L., and Stevens, Joseph E.: Flight Determination of the Drag and Longitudinal Stability and Control Characteristics of a Rocket-Powered Model of a 60° Delta-Wing Airplane from Mach Numbers of 0.75 to 1.70. NACA RM L51I04, 1951.

4. Perkins, Edward W., and Canning, Thomas N.: Investigation of Downwash and Wake Characteristics at a Mach Number of 1.53. II - Triangular Wing. NACA RM A9D20, 1949.

CONFIDENTIAL

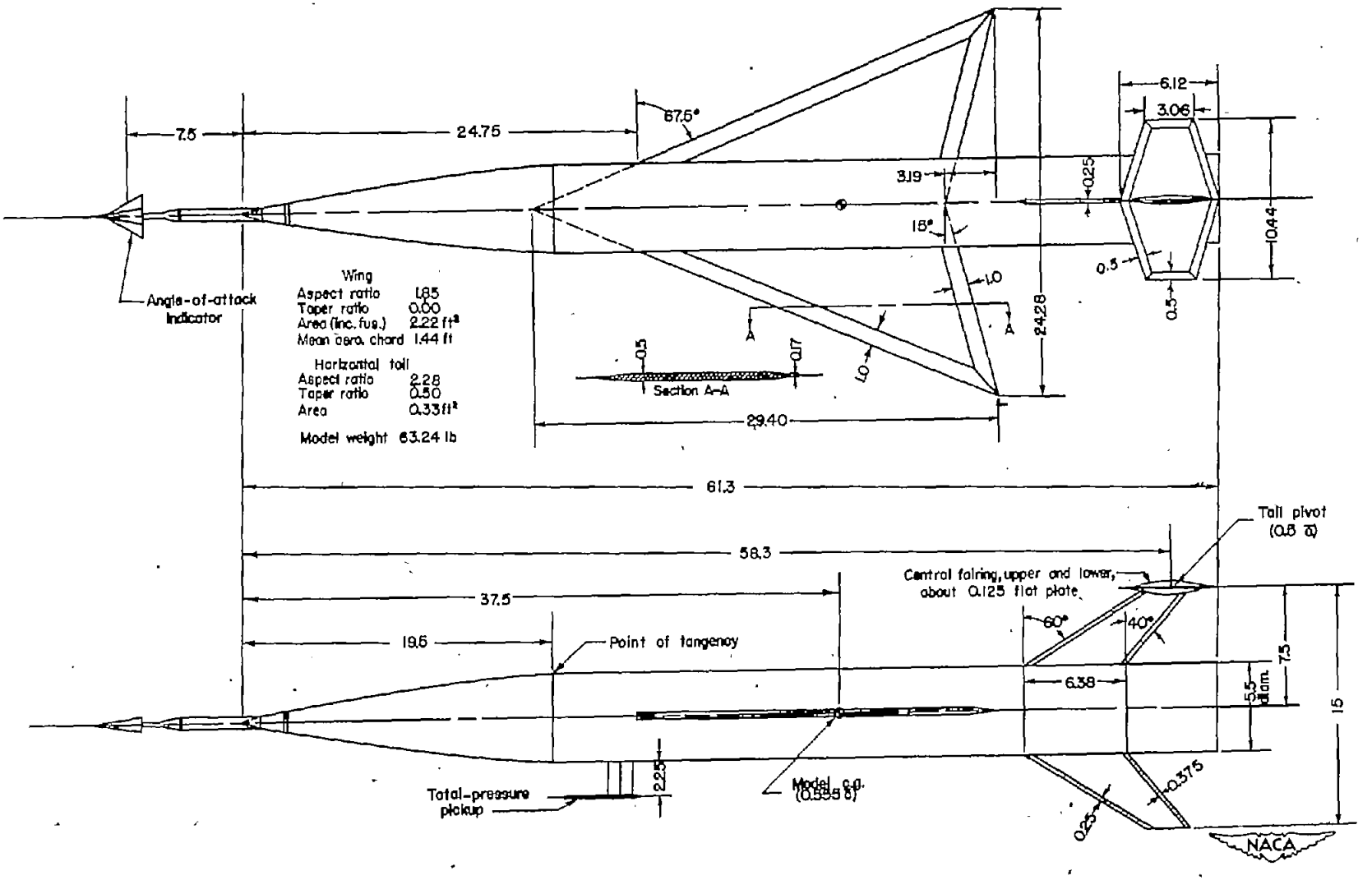

Figure 1.- Two-view drawing of test model. All dimensions in inches unless otherwise indicated.

CONFIDENTIAL

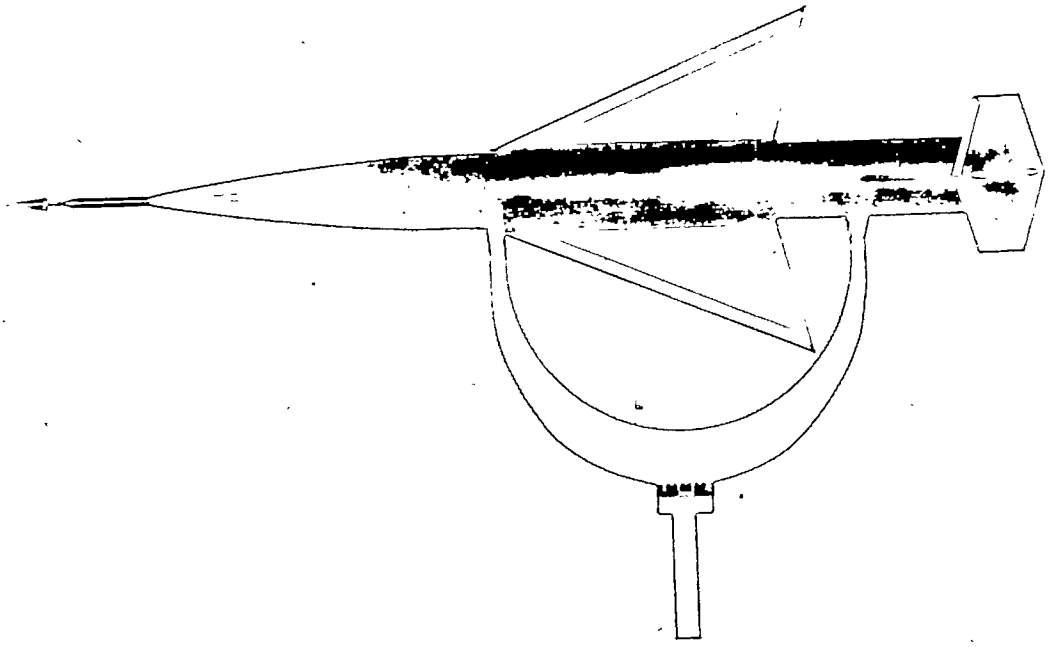

Top view

L-67414.1

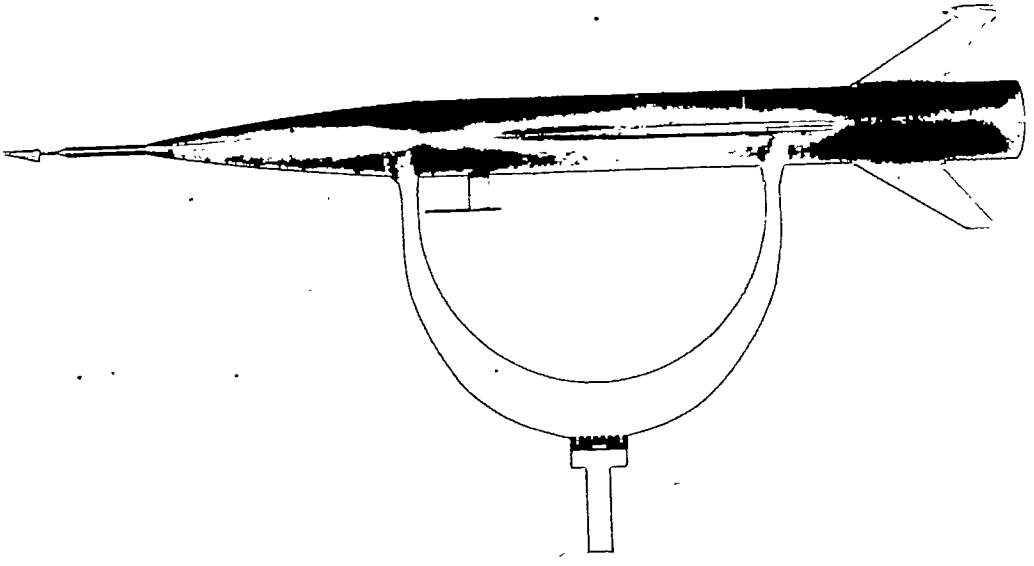

Side view

L-67415.1

Figure 2.- Photographs of test model.

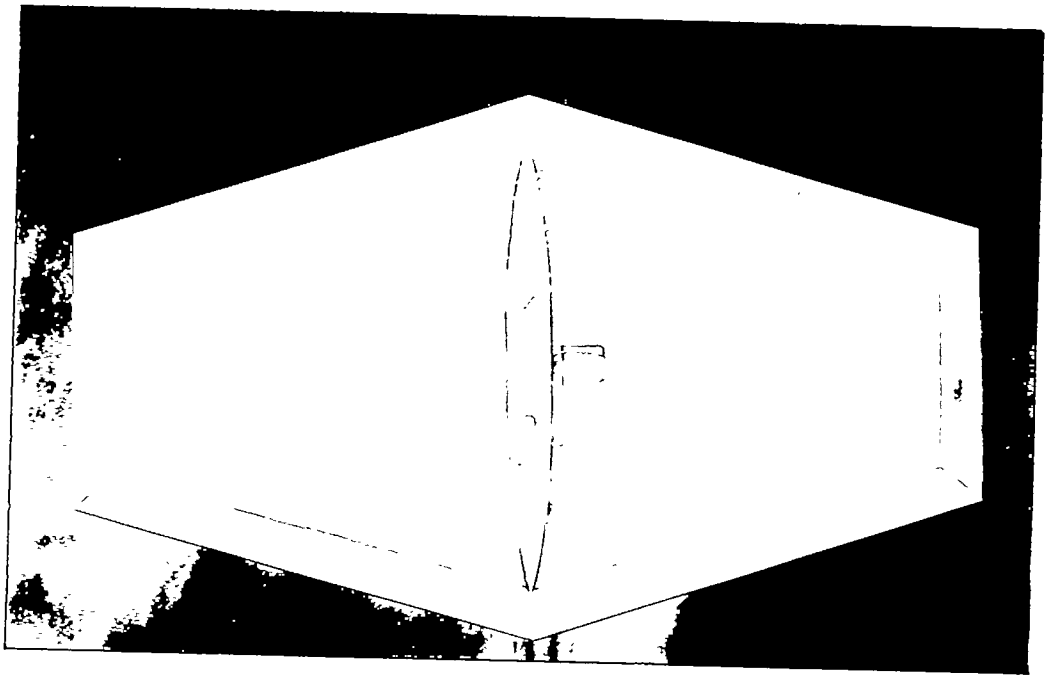

Top view

NACA
L-68613.1

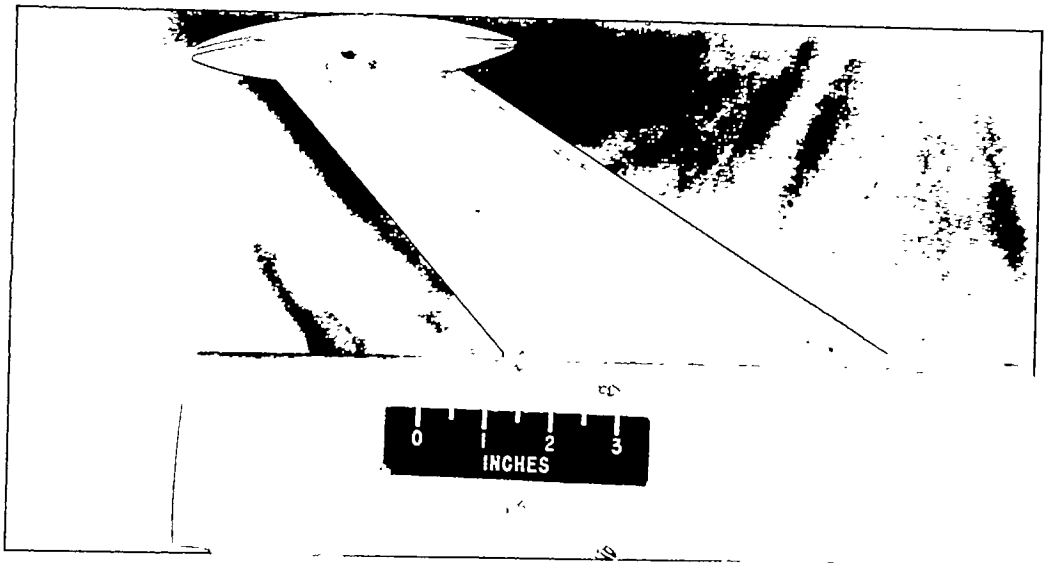

Side view

NACA
L-68614

Figure 3.- Photographs of hinged tail.

NACA
L-68754

Figure 4.- Model and booster.

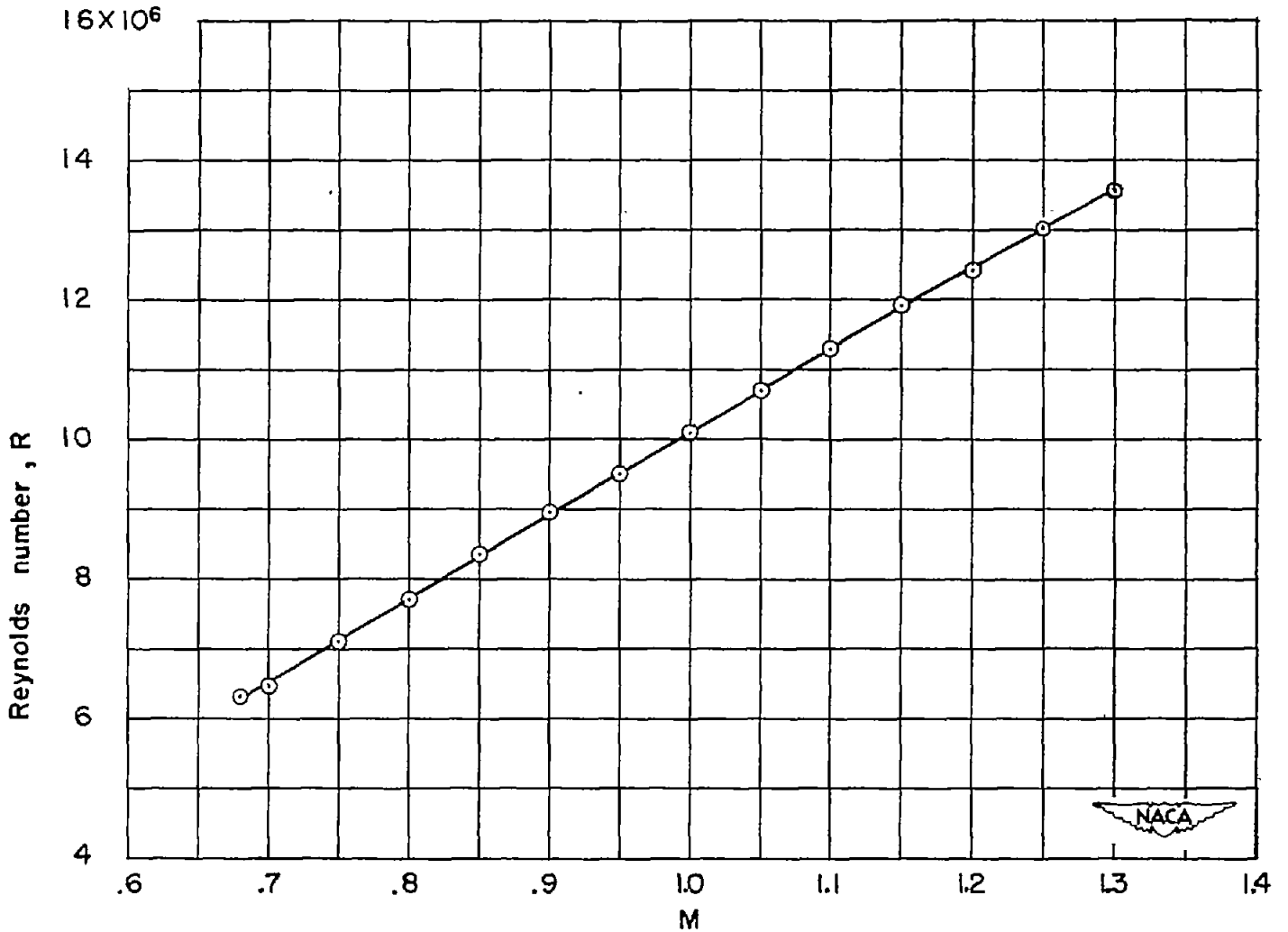

Figure 5.- Variation of test Reynolds number, based on wing mean aerodynamic chord of 1.44 feet, with Mach number.

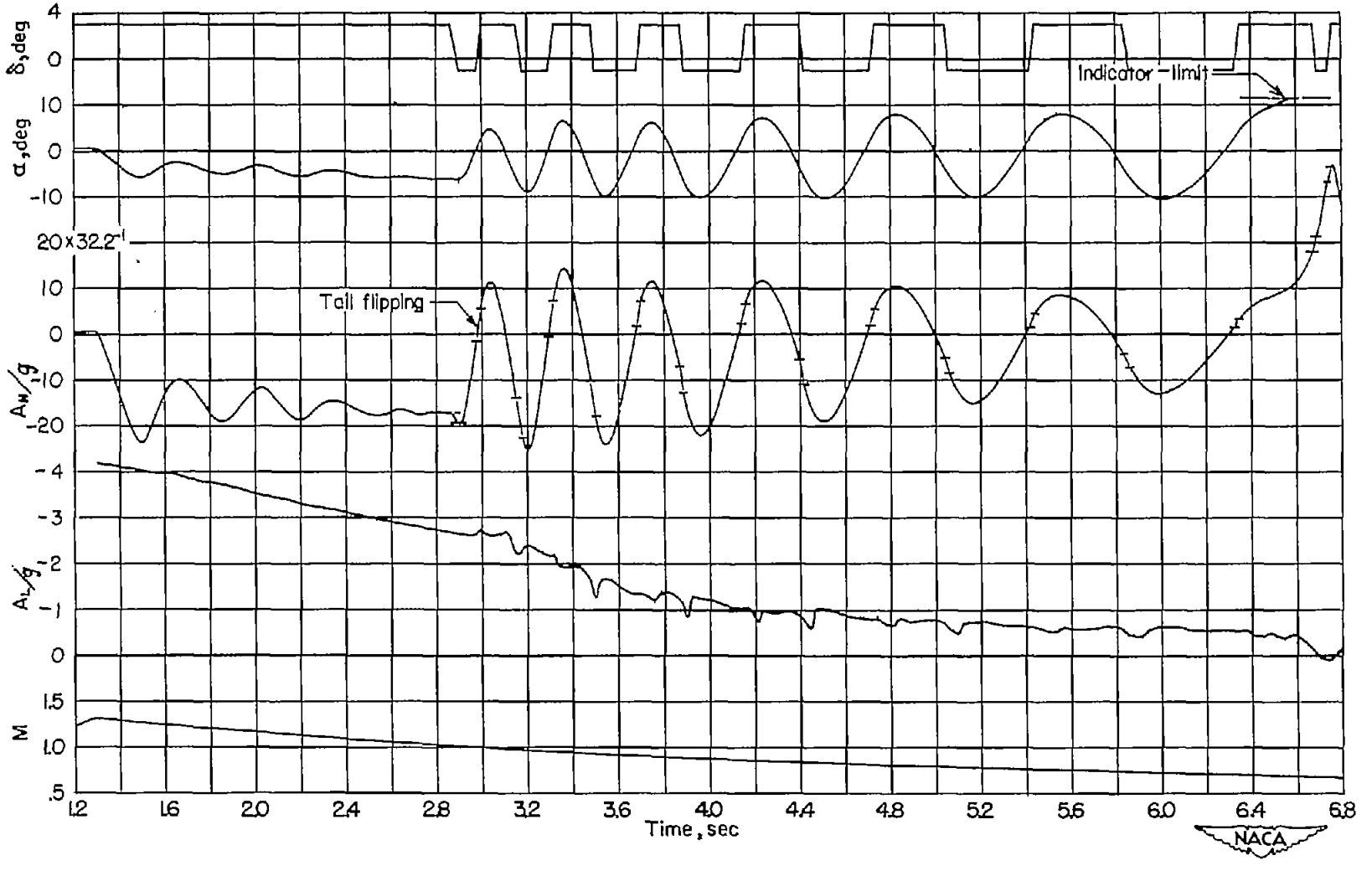

Figure 6.- Time history showing pitching oscillations of model after separation from booster.

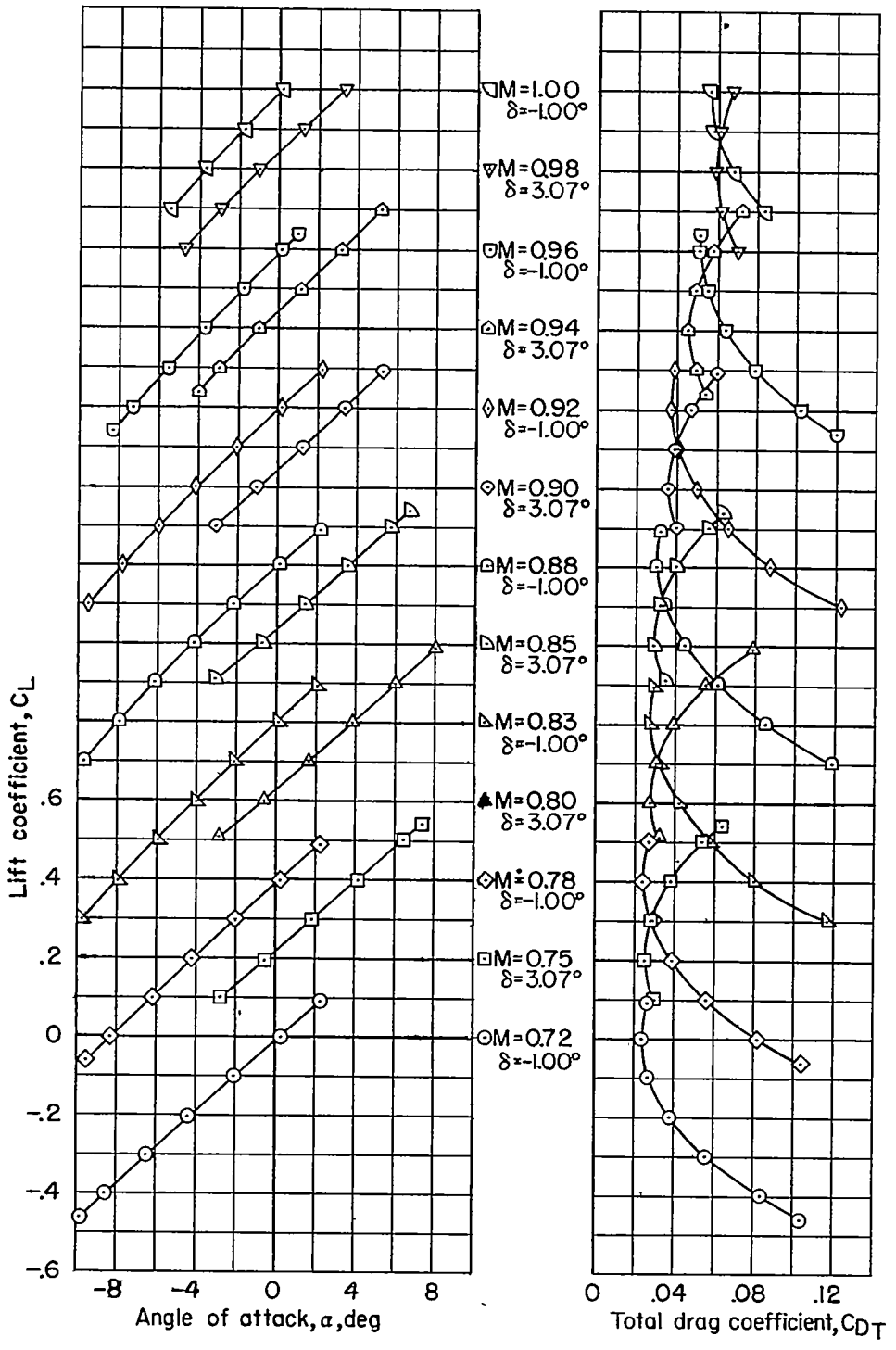

(a) During aeropulsing.

Figure 7.- Lift coefficient plotted against angle of attack and total drag coefficient.

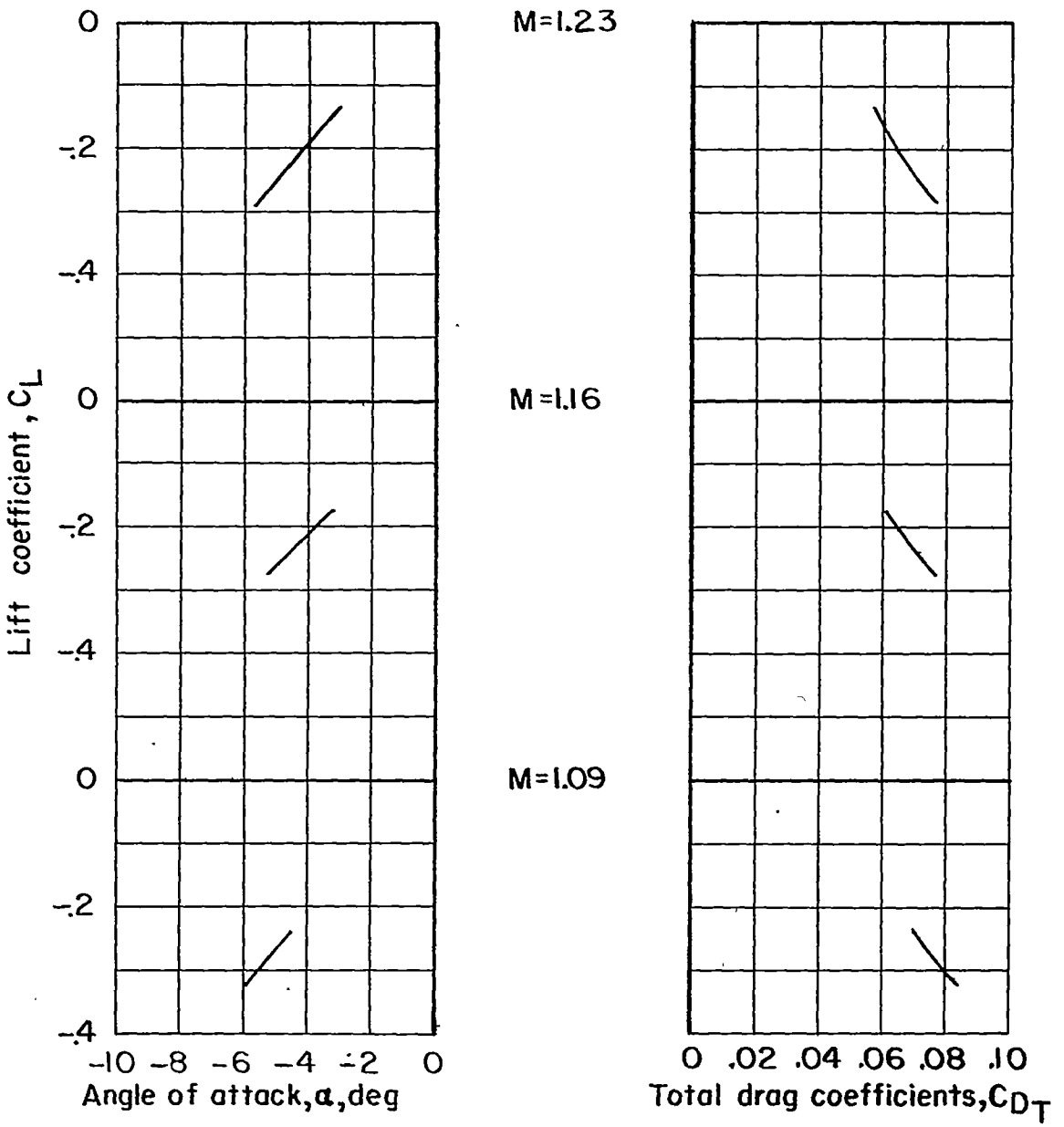

(b) During damped oscillation, $\delta = 3.07^{\circ}$.

Figure 7.- Concluded.

CONFIDENTIAL

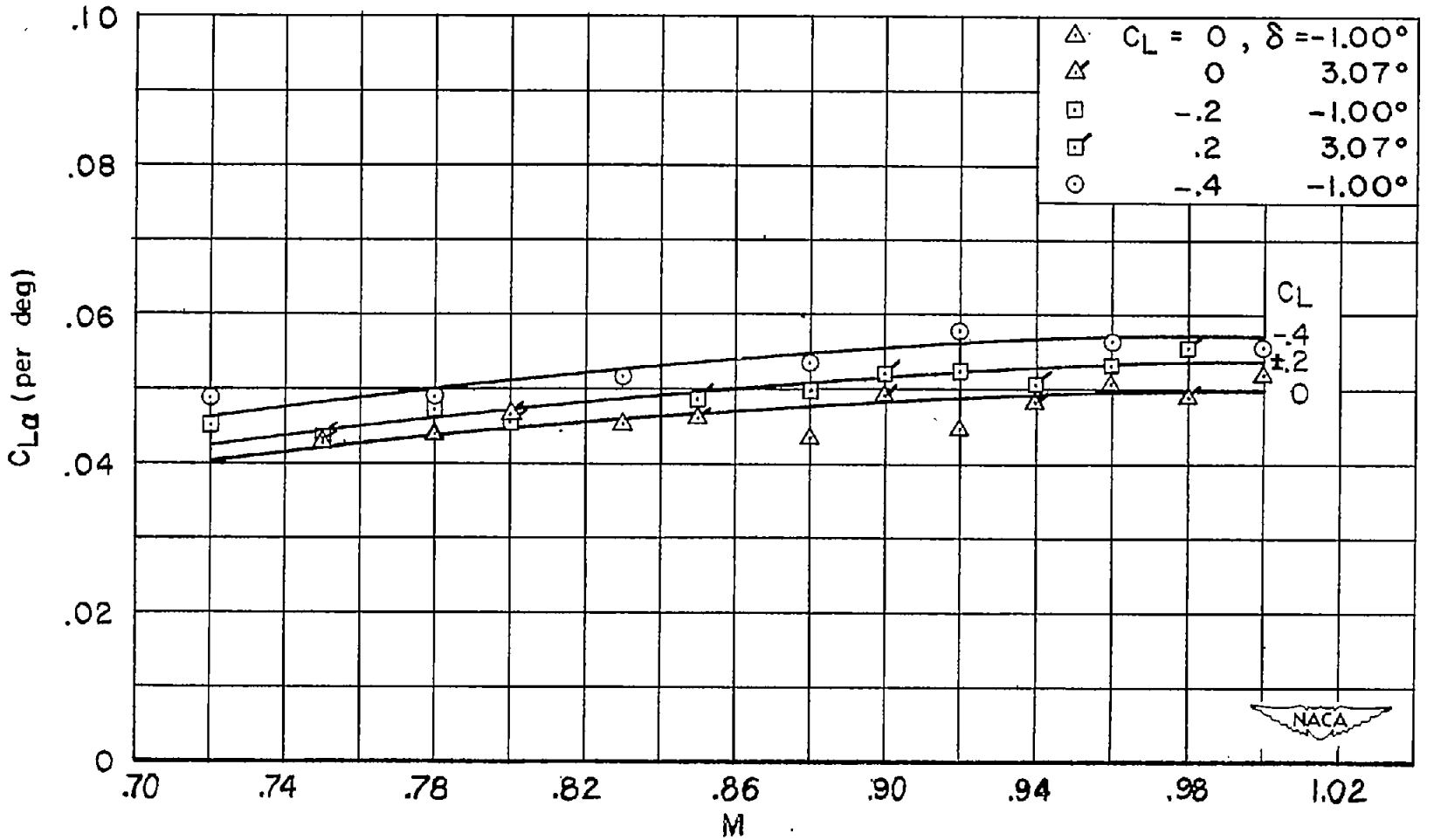

Figure 8.- Lift-curve slope against Mach number.

CONFIDENTIAL

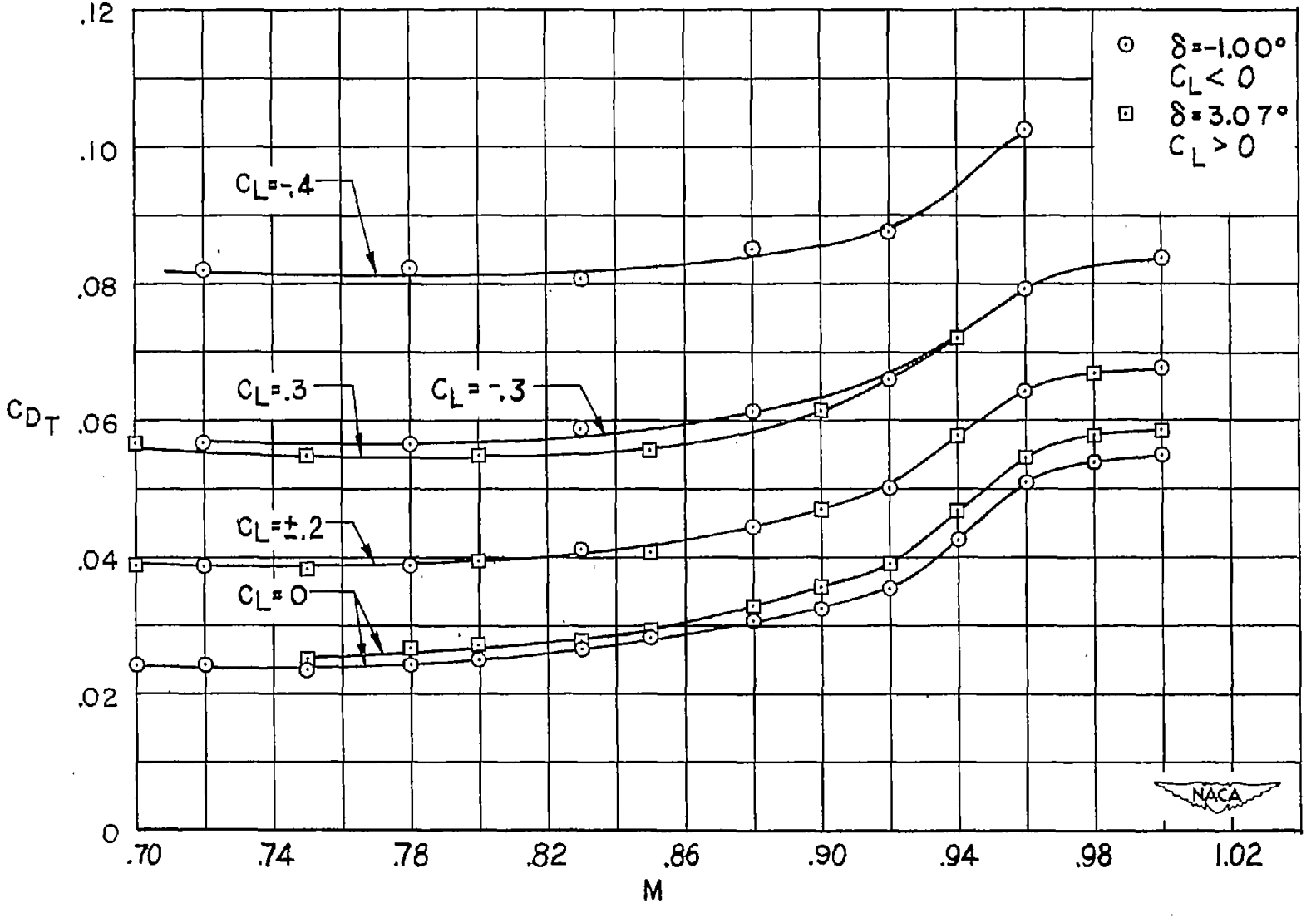

Figure 9.- Total drag coefficient against Mach number.

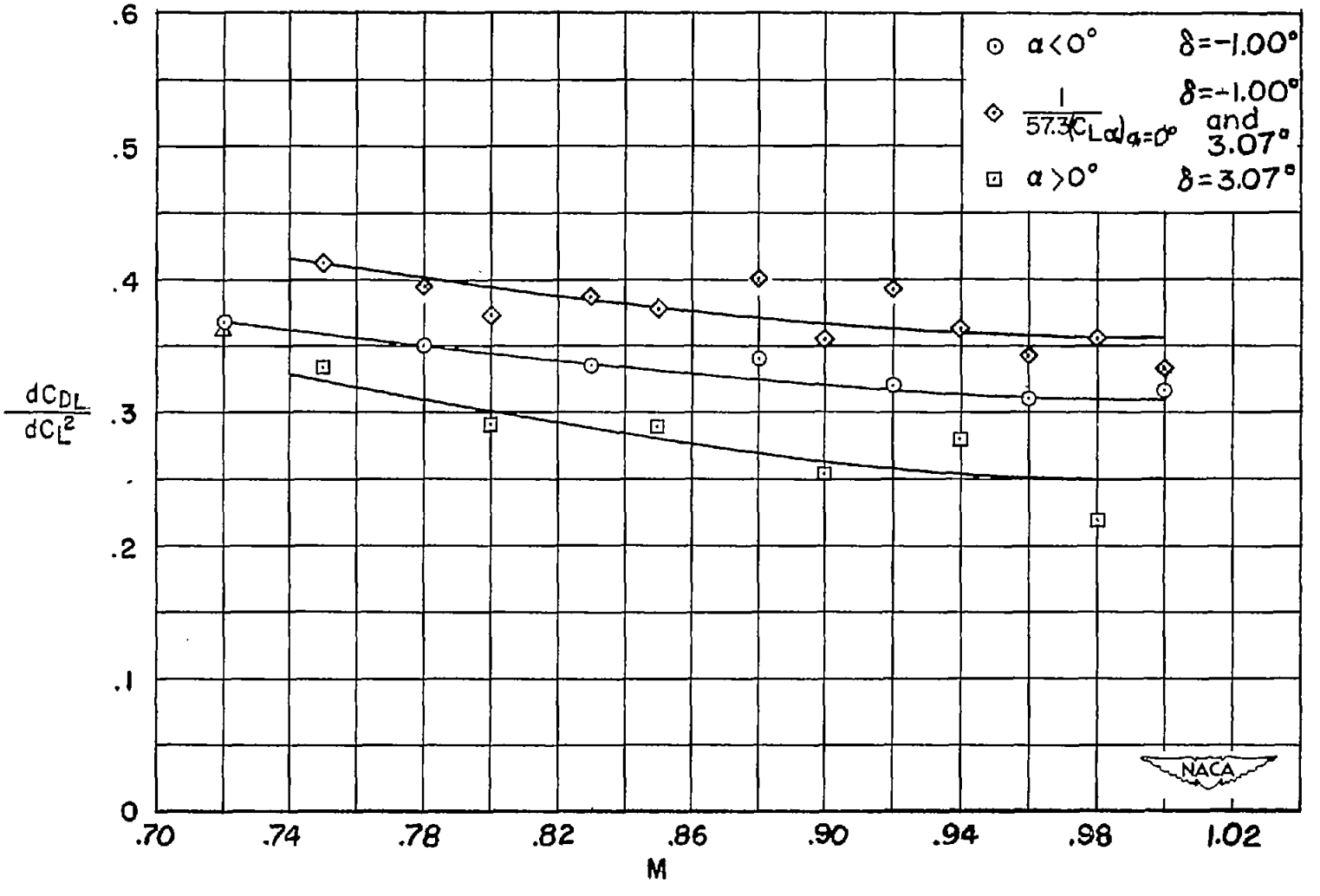

Figure 10.- Drag parameter $\frac{dC_{D_L}}{dC_L^2}$ against Mach number.

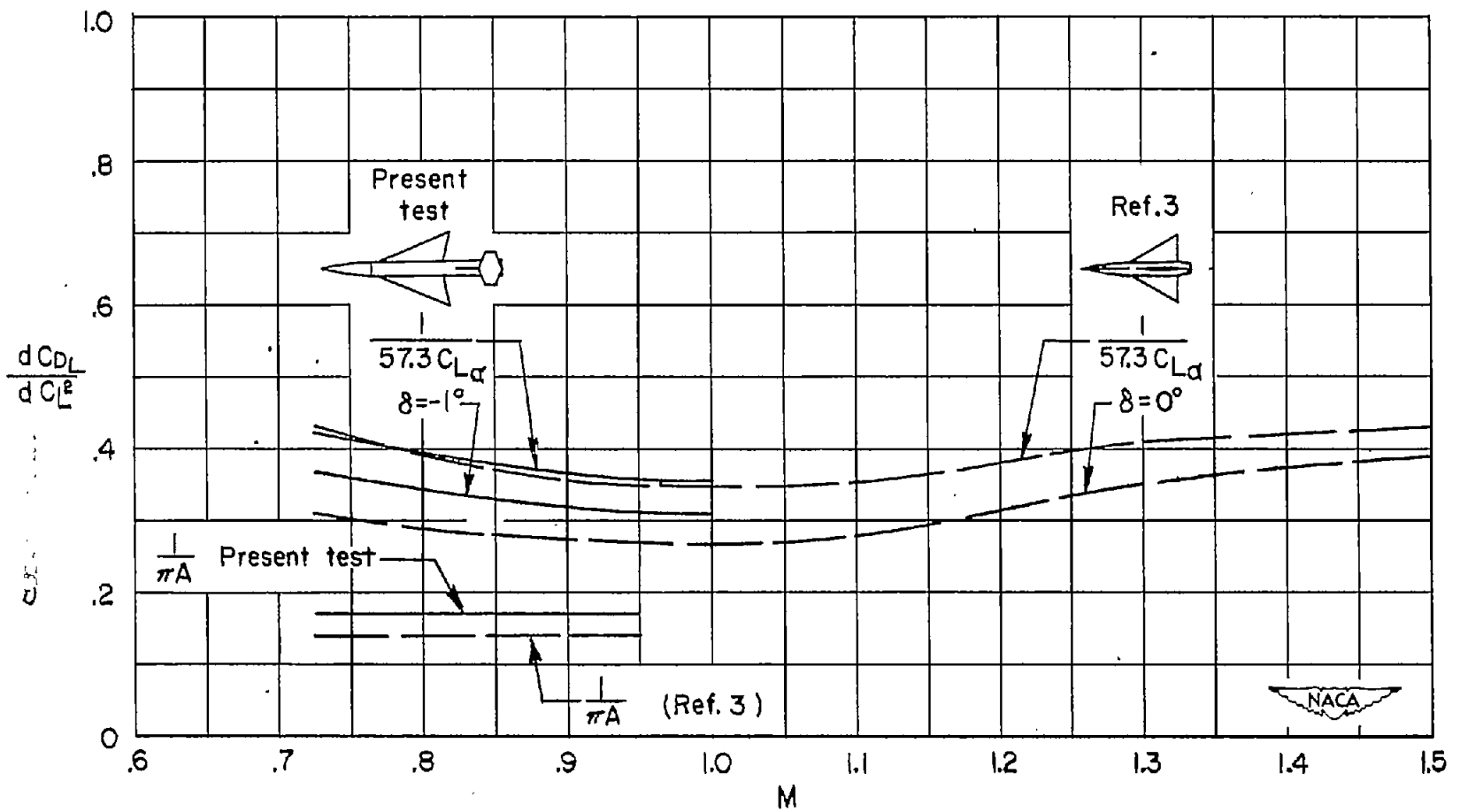

Figure 11.- Comparison of drag parameter $\frac{dC_{D_L}}{dC_L^2}$ for two similar configurations.

[redacted]

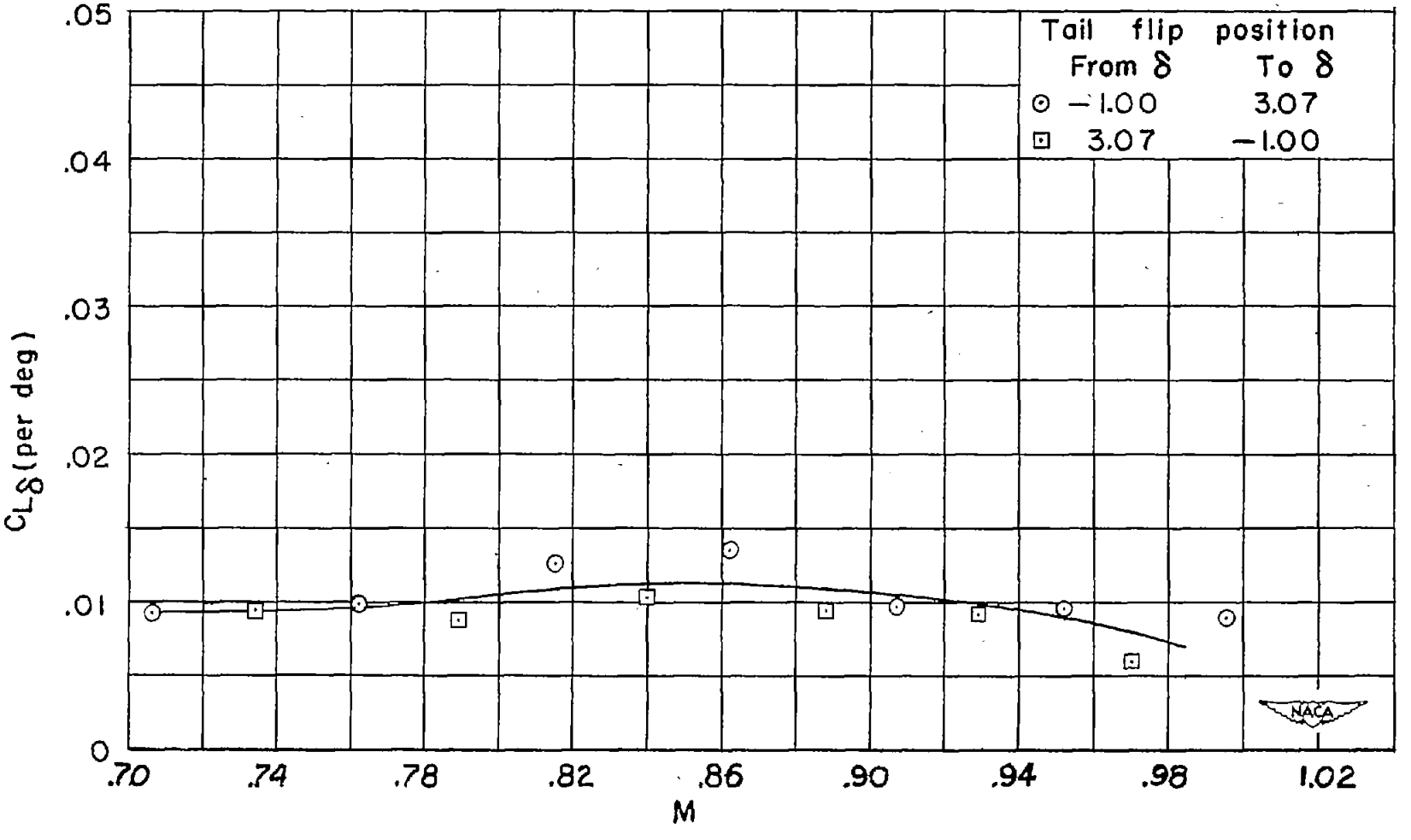

Figure 12.- Lift effectiveness of horizontal tail.

[redacted]

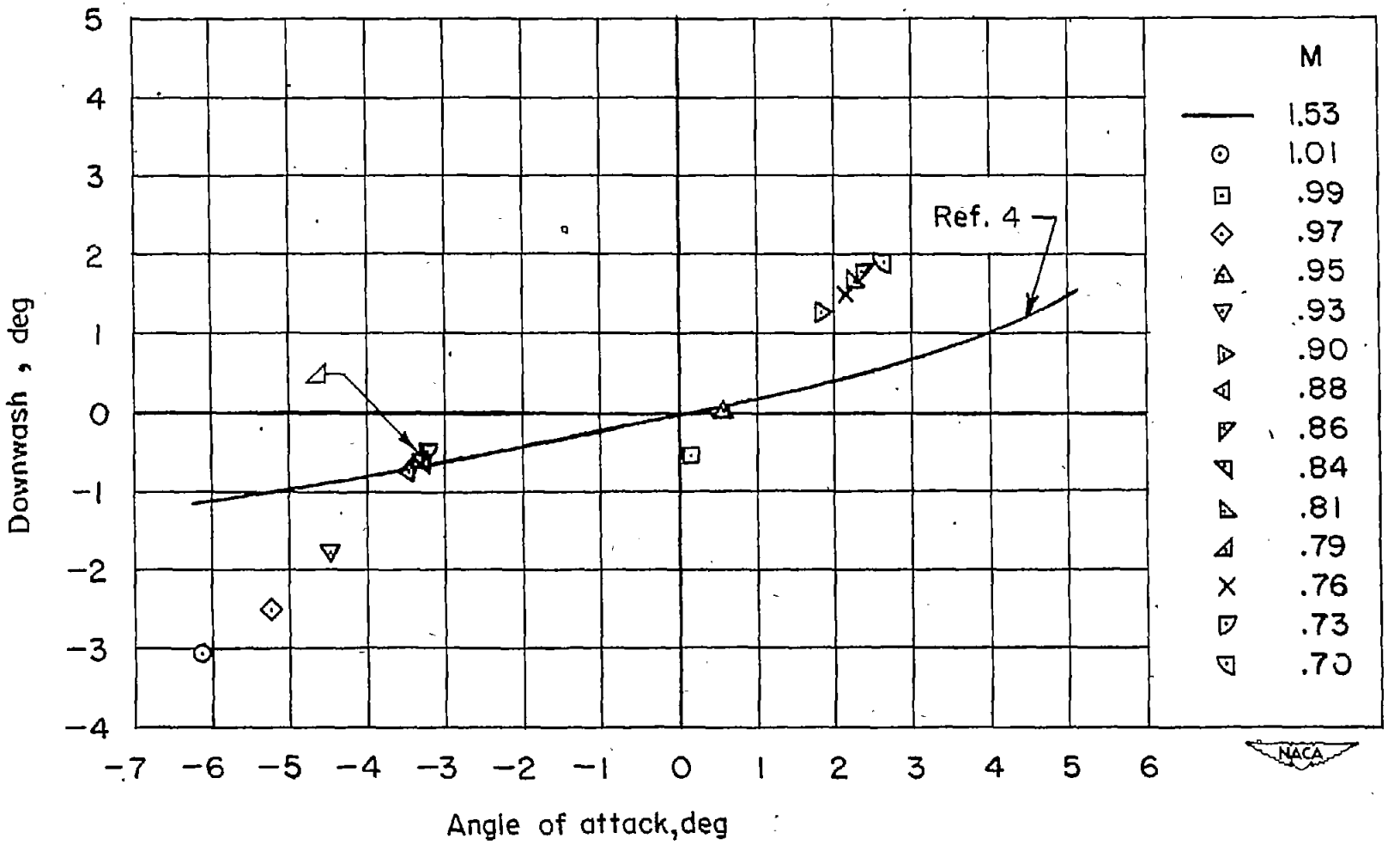

Figure 13.- Effective downwash at horizontal tail.

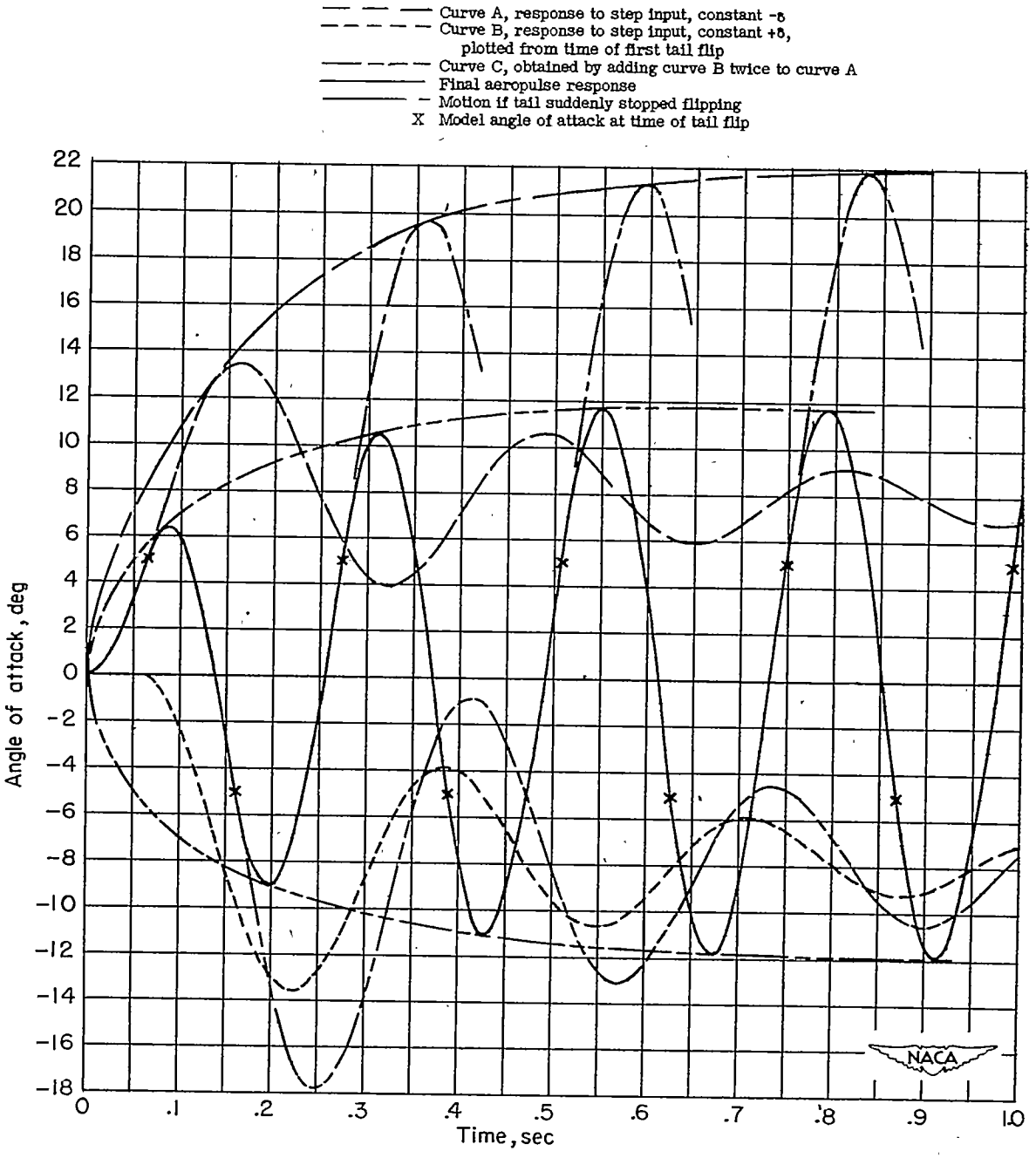

gure 14.- Graphical solution to obtain angle-of-attack response to aeropulsed tail. Mach number, 0.82; center of gravity at 20 percent mean aerodynamic chord; $\delta = \pm 3^{\circ}$; $\frac{d\epsilon}{d\alpha} = 0.40$. Configuration of reference 1.

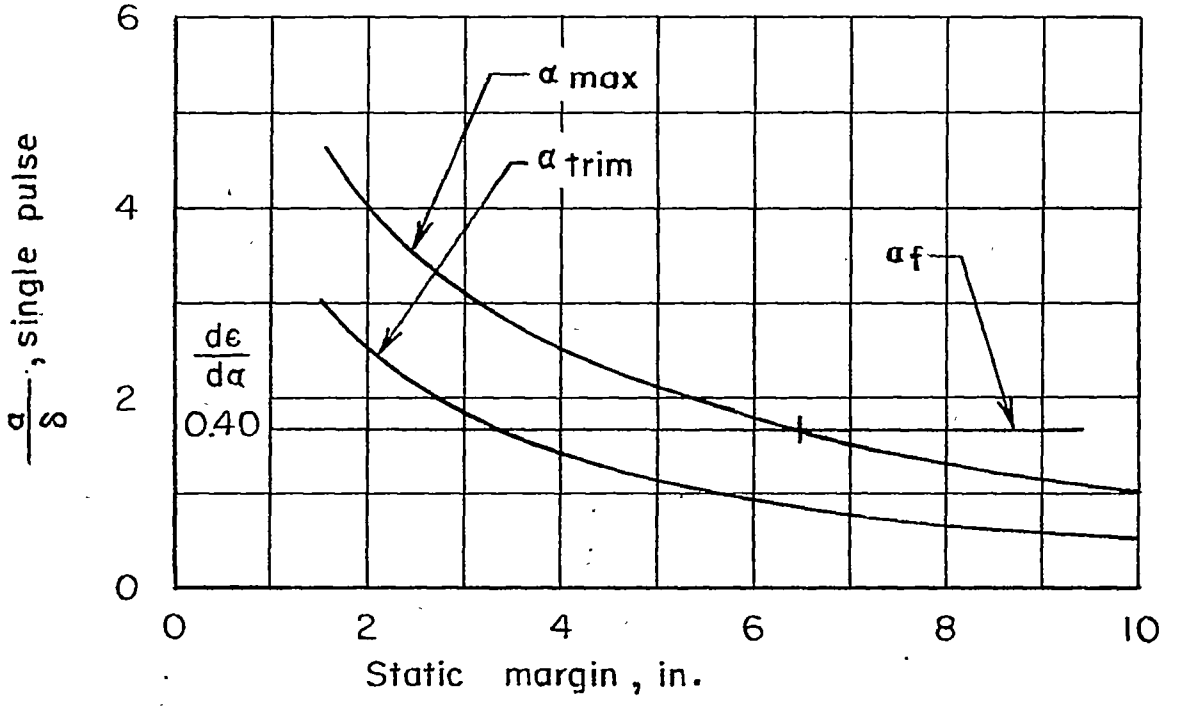

(a) α/δ response to a step input.

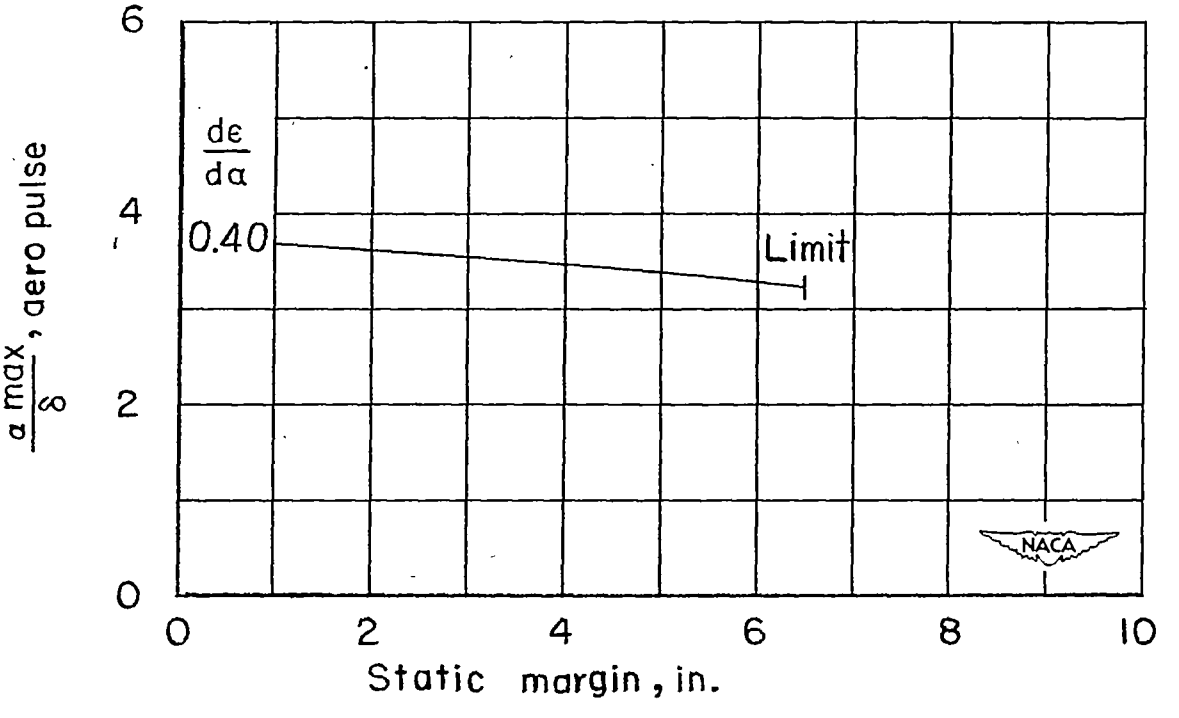

(b) α/δ response to aeropulsing.

Figure 15.- Effect of static margin on response to unit deflection of horizontal tail at Mach number 1.3. Configuration of reference 1.

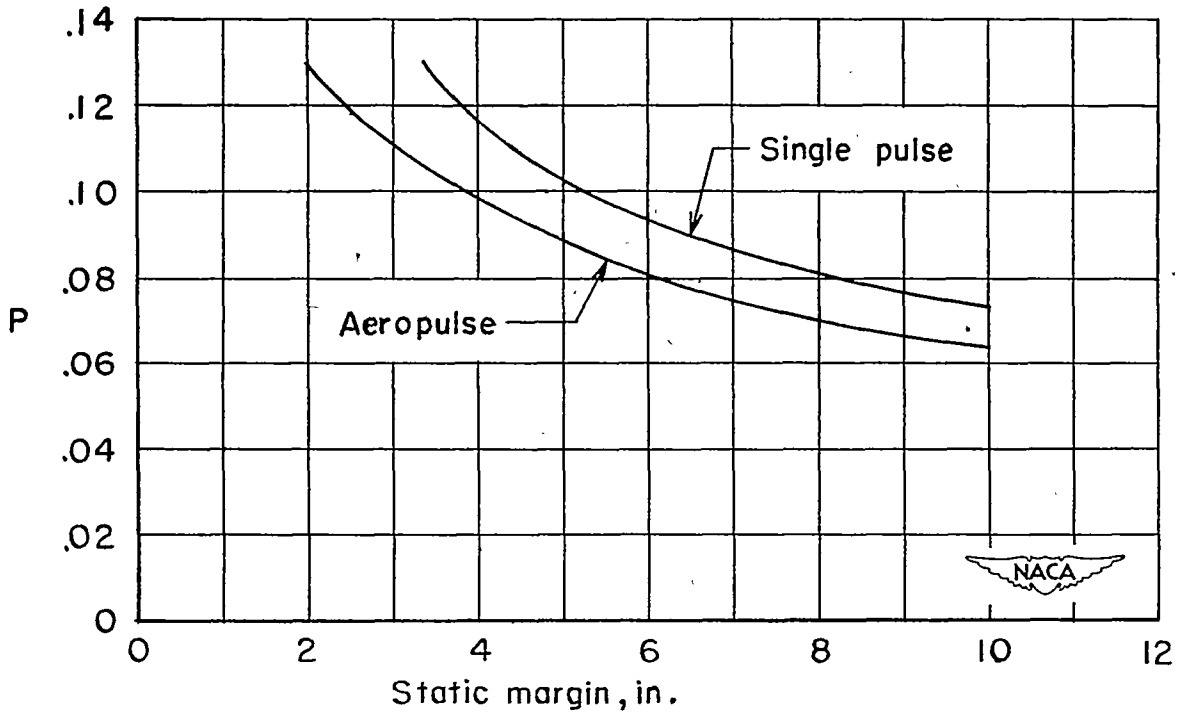

(c) Period with single pulse and aeropulse.

Figure 15.- Concluded.

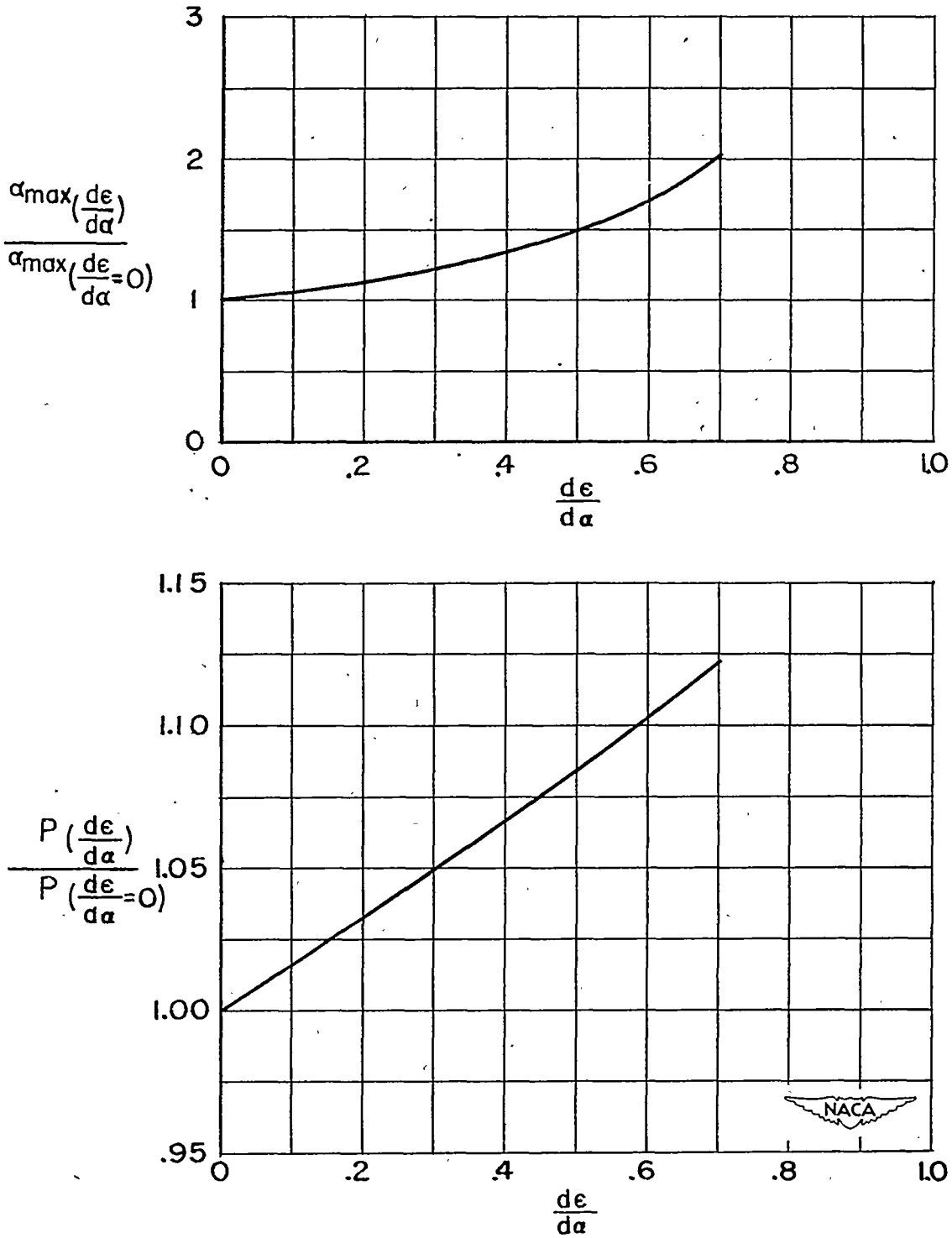

Figure 16.- Variation of α_{max} and period ratios with downwash for aeropulsing. Mach number, 1.3; center of gravity at 20 percent mean aerodynamic chord. Configuration of reference 1.

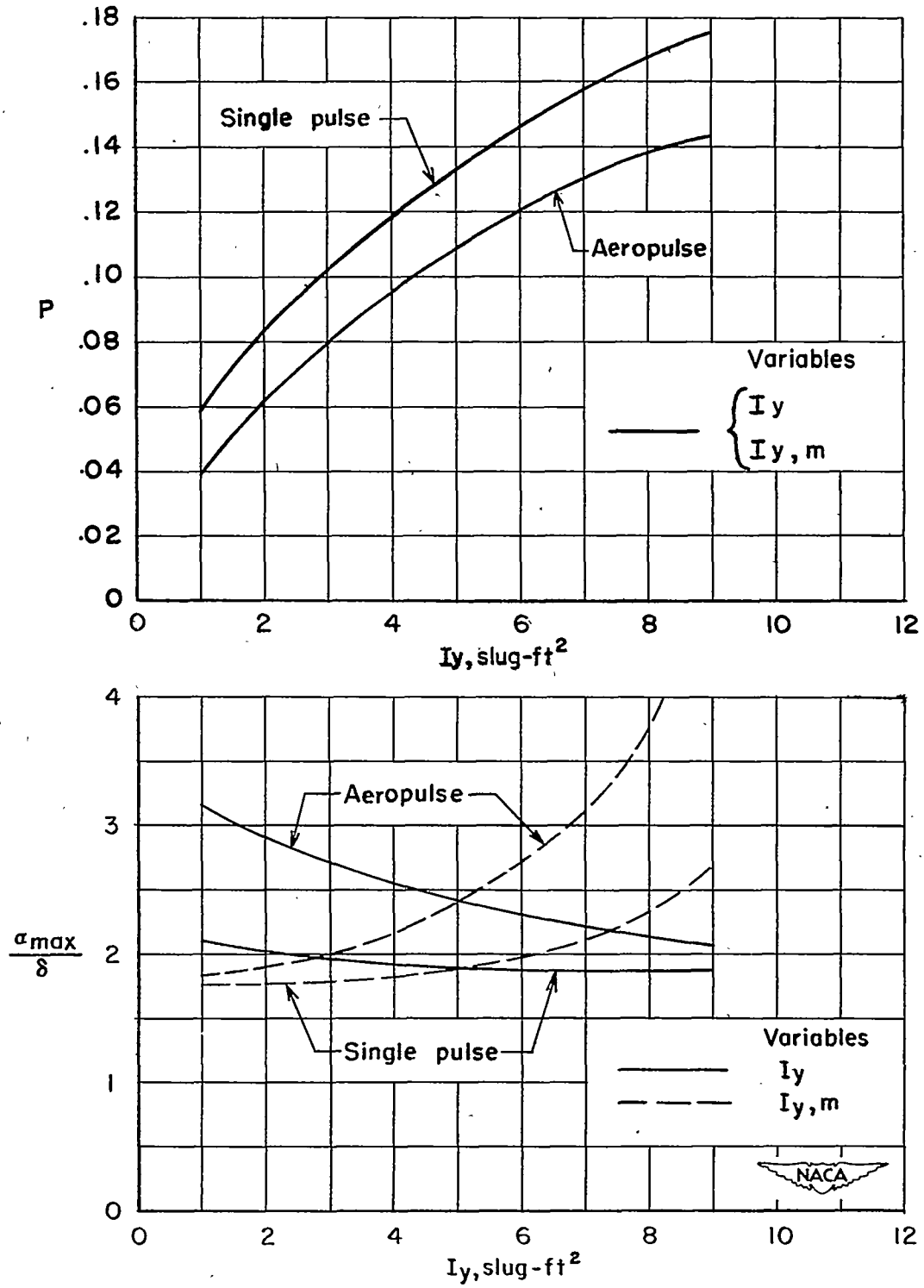

Figure 17.- Variation of α_{max}/δ and period with longitudinal inertia for step input and aeropulsing. Mach number, 1.3; center of gravity at 20 percent mean aerodynamic chord. Configuration of reference 1.